J. Micropalaeontology, 45, 377–403, 2026
https://doi.org/10.5194/jm-45-377-2026

Journal of Micropalaeontology
Open Access

Latest Guadalupian to Lopingian conodonts from western Hubei–eastern Chongqing, South China

Bingyang Zhou[1], Kui Wu[1], Teng Song[2], Lulu Xu[3], Ke Duan[3], Jinling Yuan[1], Liangzhe Yang[1], Bi Zhao[1], Jiangli Li[1], Di Wang[1], and Boyong Yang[1]

[1]Hubei Key Laboratory of Resource and Eco-Environment Geology, Hubei Institute of Geosciences, Hubei Geological Bureau, Wuhan, 430034, China
[2]Oil and Gas Survey, China Geological Survey, Beijing 100083, China
[3]Hubei Geological Survey, Wuhan 430034, China

Correspondence: Kui Wu (kuiwu@cug.edu.cn) and Boyong Yang (boyongyang@163.com)

Received: 24 December 2025 – Revised: 10 April 2026 – Accepted: 28 April 2026 – Published: 18 May 2026

Abstract. The Lopingian stratigraphic framework of the western Hubei–eastern Chongqing (WHEC) area, South China, remains insufficiently constrained, particularly regarding the precise age of the organic-rich intervals within the Dalong Formation that are considered to be favorable for shale gas exploration. To address this issue, a refined conodont biostratigraphic framework is established based on systematic sampling of the Longmenba, Huangping, and Tongmuyuan sections. A total of 17 conodont species belonging to four genera (*Jinogondolella*, *Clarkina*, *Hindeodus*, and *Iranognathus*) are identified, allowing recognition of a near-continuous succession spanning the late Wuchiapingian to the Changhsingian. Integration of biostratigraphic and lithostratigraphic data allows placement of the Wuchiapingian–Changhsingian boundary within the upper part of the Dalong Formation, with minor local variations attributable to facies differences and preservation potential. Importantly, the organic-rich, siliceous-shale interval in the lower Dalong Formation is shown to be temporally restricted to the late Wuchiapingian, mainly corresponding to the upper *Clarkina guangyuanensis* Zone and extending into the *C. orientalis* or lowermost *C. longicuspidata* Zone. The temporal overlap between late Wuchiapingian conodont zones, regional basin deepening, and waning eruptive phases of the Emeishan Large Igneous Province suggests broader tectono-environmental controls on sedimentary and biotic evolution. This study highlights the value of high-resolution conodont biostratigraphy in resolving Lopingian depositional history and in linking micropaleontological records with regional paleoenvironmental change.

1 Introduction

The Permian Period represents one of the most critical chapters in Earth history, marked by profound biological, climatic, and tectonic transformations, including the assembly of Pangea, long-term climate transition from icehouse to greenhouse conditions, emplacement of large igneous provinces, and end-Guadalupian and end-Permian mass extinctions (Wignall et al., 2009; Shen et al., 2019; Fan et al., 2020; Zhang et al., 2025a). These global-scale processes exerted a fundamental control on marine ecosystem evolution and sedimentary basin development, thereby influencing the distribution of mineral and energy resources (Shen et al., 2019; Guo et al., 2025).

As a tectonically stable and relatively isolated continental block along the eastern margin of the Paleo-Tethys Ocean (Fig. 1a), the South China Block (SCB) preserves one of the most complete and continuous Permian marine successions worldwide (Shen et al., 2019). Three Global Stratotype Section and Points (GSSPs) have been established within this region (Yin et al., 2001; Jin et al., 2006a, b). These successions provide an exceptional archive of the end-Guadalupian and end-Permian mass extinctions, together with their associated volcanism, climatic perturbations, and sedimentary responses (Wignall et al., 2009; Shen et al., 2019). The eruption

of the Emeishan Large Igneous Province (LIP) is widely considered to be a principal trigger of the end-Guadalupian biotic crisis; both the silicic eruption phase (Yang et al., 2015) and subsequent weathering (Viaretti et al., 2025; Gong et al., 2025) of the volcanic province have been proposed to induce short-term climatic perturbations, including transient global cooling. In addition to their paleoenvironmental significance, these strata host important mineral and hydrocarbon resources, including bauxite, manganese deposits, and organic-rich shales with significant shale gas potential (Shen et al., 2019; Meng et al., 2022; Guo et al., 2025).

The western Hubei–eastern Chongqing (WHEC) area contains thick Lopingian marine successions, including the Dalong Formation, which hosts organic-rich siliceous shales regarded to be promising shale gas targets. Recent exploration has confirmed substantial shale gas reserves in this region (Qiu et al., 2024; Xu et al., 2025; Yong et al., 2025). However, despite its economic importance, the chronostratigraphic framework of the Upper Permian in the WHEC area remains insufficiently resolved. In particular, the precise temporal position and regional synchronicity of the organic-rich shale interval within the Dalong Formation are poorly constrained. Existing correlations are largely lithostratigraphic and lack high-resolution biostratigraphic control, leading to uncertainty in evaluating whether shale-gas-favorable horizons are time-equivalent across different sections.

To resolve these issues, this study undertakes systematic conodont sampling from representative Lopingian sections in the WHEC area. By establishing a refined conodont biostratigraphic framework and integrating it with lithostratigraphic observations, we aim to constrain the geological age of shale-gas-bearing intervals and to provide a robust chronostratigraphic basis for regional correlation and resource assessment.

2 Geological settings

During the Permian, the SCB was situated along the eastern margin of the Paleo-Tethys Ocean (Fig. 1a), where extensive marine sedimentation took place, including siliceous, clastic, and carbonate deposits. The eruption of the Emeishan flood basalts, in combination with the Dongwu tectonic uplift and a global eustatic sea level regression, resulted in the development of a regionally extensive unconformity across South China. This unconformity represents a key stratigraphic marker separating the Guadalupian and Lopingian successions (Yuan et al., 2017; Shen et al., 2019; Hou et al., 2020). Prior to this unconformity, several intra-shelf basins had developed within the shallow-marine carbonate platform of the SCB (Qiu et al., 2024). Regionally, the shallow-water platform facies are represented by the Guadalupian Maokou Formation (Fig. 2a), whereas contemporaneous deep-water deposits are typified by the Gufeng Formation (Fig. 2a–c). Following the regression, the western margin of the SCB, including the WHEC area, evolved into a transitional setting between shallow carbonate platforms and deeper intra-shelf basins (Fig. 1b). This paleogeographic configuration was conducive to the accumulation of thick, organic-rich black shales, which now constitute important shale gas reservoirs (Guo et al., 2025; Yong et al., 2025).

The Upper Permian succession in the WHEC area comprises, in ascending order, the Longtan, Xiayao, and Dalong formations. The Longtan Formation is composed mainly of tuffaceous arenite and sandy mudstone (Fig. 2c–d), whereas the Xiayao Formation is dominated by dark-gray, medium-bedded limestones (Fig. 2d–e). The overlying Dalong Formation is characterized by bedded chert, siliceous mudstone, and muddy limestone (Fig. 2f–h). Together, these formations record pronounced paleoenvironmental changes associated with both the end-Guadalupian and end-Permian crises and also represent key stratigraphic intervals of unconventional hydrocarbon exploration (e.g., Yong et al., 2025; Zhang et al., 2025b; Xu et al., 2025). The Dalong Formation is overlain by the first member of the Daye Formation, which consists mainly of thin-bedded mudstone and marly limestone (Xu et al., 2025). In some shallow-water facies, the top of the Dalong Formation is marked by medium-thick limestones containing siliceous nodules. The uppermost Dalong Formation is marked by medium- to thick-bedded limestones containing siliceous nodules. Microbialite buildups commonly occur at the transition between these limestones and the overlying thin-bedded mudstones of the Daye Formation. Recent studies indicate that these microbialites in western Hubei are of earliest Triassic age (Du et al., 2025).

Five representative stratigraphic sections were investigated in this study: Longmenba, Chenjiawan, Longjingwan, Huangping, and Tongmuyuan, all located within the middle Yangtze region of South China (Fig. 1c). The Longmenba section (30°31′36″ N, 109°22′12″ E), near Longqiao Town, Fengjie County (Chongqing), is well exposed and has previously been studied for its Dalong Formation paleoenvironmental record (Xu et al., 2025). The Huangping (30°03′17″ N, 109°26′07″ E) and Tongmuyuan (29°40′11″ N, 109°37′21″ E) sections are located in Jiaoyuan and Shadaogou towns, Xuan'en County (Hubei Province). The Chenjiawan (30°09′33″ N, 109°01′57″ E) and Longjingwan (30°06′08″ N, 108°52′41″ E) sections occur in Shaxi and Yuanbao towns, Lichuan County, Hubei Province. All five sections expose the entire or partial Upper Permian Dalong and Xiayao Formations, whereas the Longjingwan and Longmenba sections additionally include the Upper Permian Longtan Formation and the Guadalupian Gufeng and Maokou Formations (Fig. 3).

3 Materials and methods

Because certain intervals of the Dalong and Gufeng formations contain high proportions of siliceous or argillaceous

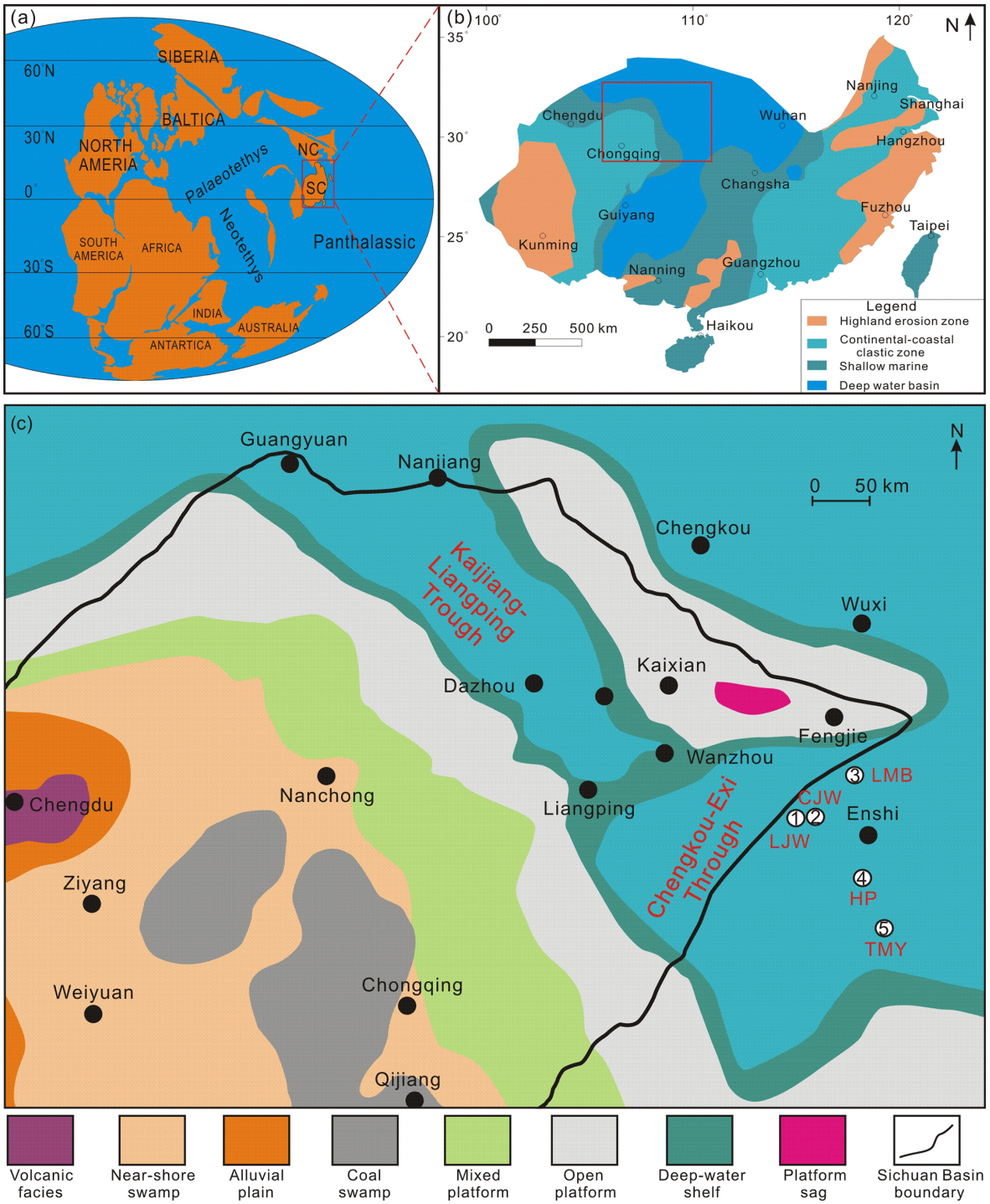

Figure 1. Locations of the studied sections in the WHEC area. **(a)** Paleogeographic reconstruction near the Guadalupian–Lopingian boundary (modified after Hou et al., 2020). SC stands for South China; NC stands for North China. **(b)** Paleogeographic reconstruction for the late Wuchiapingian (modified after Hou et al., 2020). **(c)** Sedimentary facies distribution of the Dalong Formation of the WHEC area (modified after Yong et al., 2025). LJW stands for Longjingwan, CJW stands for Chenjiawan, LMB stands for Longmenba, HP stands for Huangping, and TMY stands for Tongmuyuan.

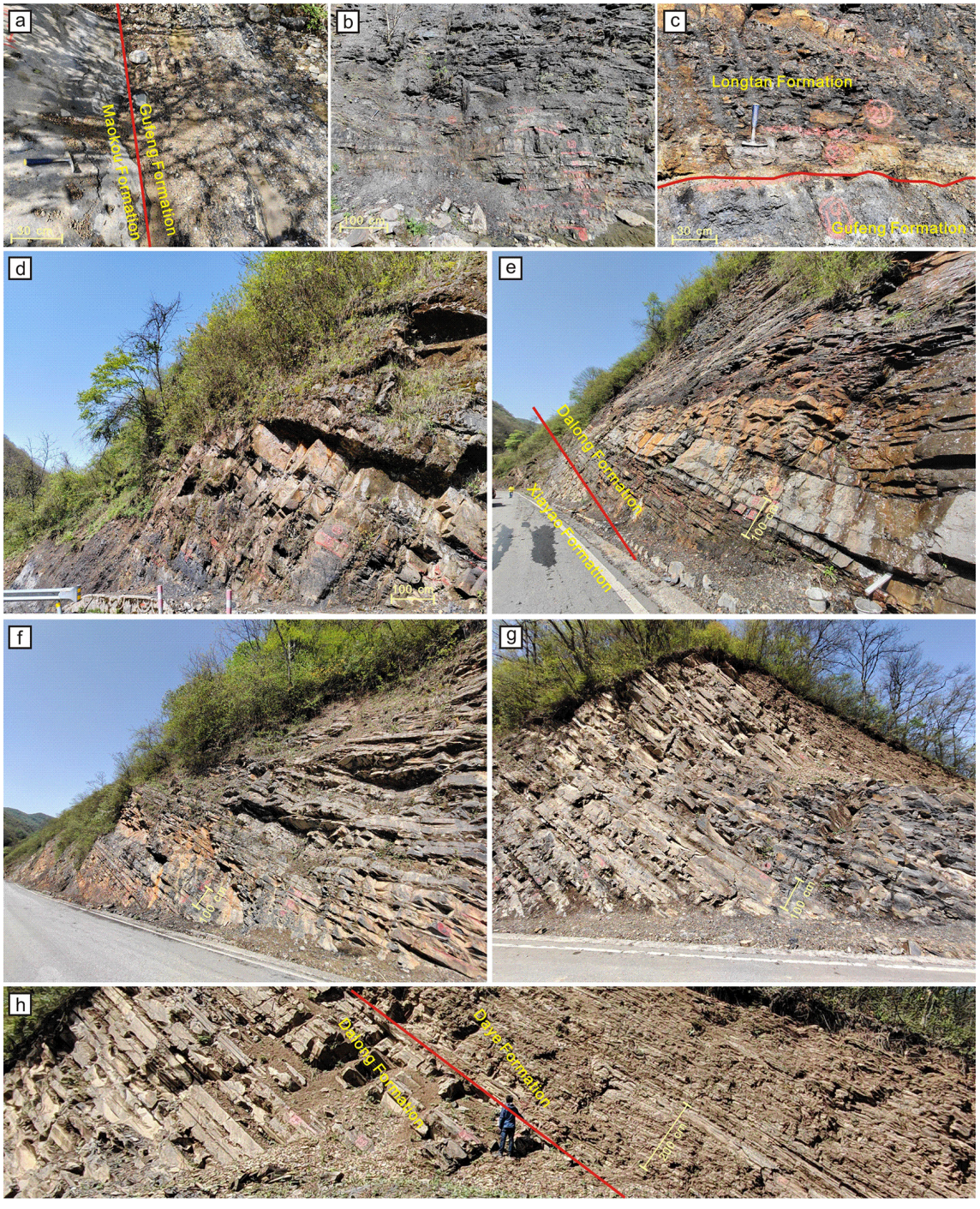

Figure 2. Field photographs of the Longmenba section. **(a)** Light-gray thick-bedded limestone of the topmost Maokou Formation, overlain by dark-gray, thin-bedded chert with limestone of the Gufeng Formation. **(b)** Dark-gray, thin-bedded siliceous shale from the upper part of the Gufeng Formation. **(c)** Siliceous shale from the Gufeng Formation and clastic rocks from the basal Longtan Formation; note the development of a yellowish volcaniclastic sandstone between the two formations. **(d)** Sandstone from the upper part of the Longtan Formation. **(e)** Thin- to medium-bedded limestone of the Xiayao Formation, overlain by thin-bedded chert with limestone of the lower Dalong Formation. **(f)** Thin-bedded argillaceous limestone and mudstone with limestone nodules from the upper part of the Dalong Formation. **(g)** Thin-bedded mudstone and argillaceous limestone from the uppermost part of the Dalong Formation. **(h)** Thin-bedded mudstone of the Dalong Formation overlain by muddy shales from the Daye Formation.

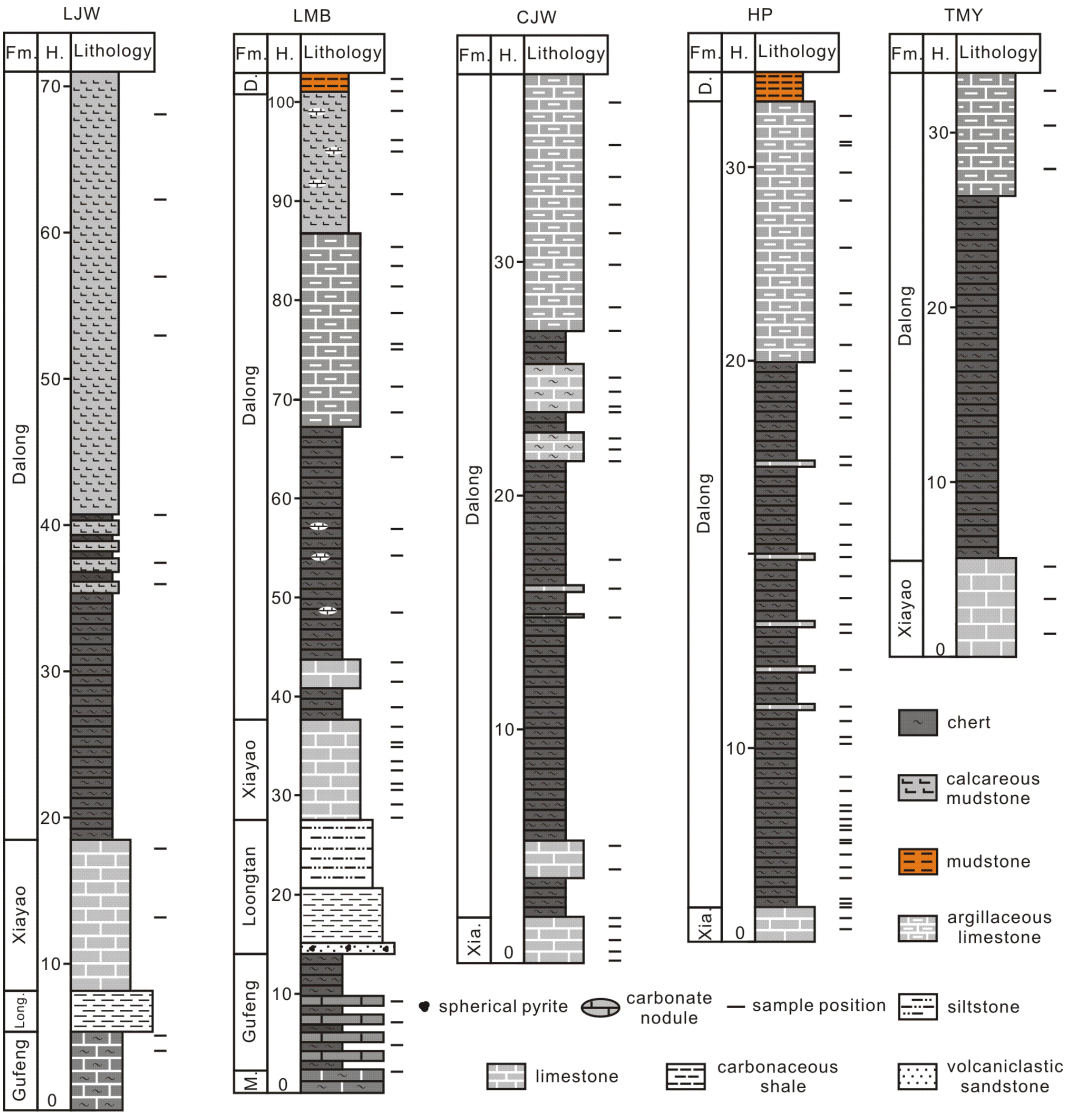

Figure 3. Lithology, stratigraphic ranges, and sample positions of the studied sections.

material that are unsuitable for conodont extraction using the acetic acid method, field sampling focused primarily on lithologies that readily react with dilute hydrochloric acid. Stratigraphic coverage and sampling resolution were also carefully considered to ensure representative coverage of different stratigraphic levels. In total, 127 limestone and calcareous mudstone samples were collected, including 25 from the Chenjiawan section, 11 from Longjingwan, 45 from Huangping, 34 from Longmenba, and 6 from Tongmuyuan. In the laboratory, samples were initially crushed into fragments approximately 3–5 cm in size and placed in plastic buckets. A 10 % acetic acid solution was then added and allowed to react for 1–2 d. After the initial reaction had subsided, the supernatant was carefully decanted and replaced with fresh acid solution added along the bucket walls to minimize disturbance of the residues. This procedure was repeated over a total reaction period of 7–10 d. Upon completion of dissolution, the residues were wet-sieved through a 20-mesh sieve, with a 160-mesh sieve placed beneath it. The fine residues retained on the lower sieve were gently washed, collected, and air-dried. Any remaining undissolved material was returned to the bucket for further acid treatment until dissolution was complete. Heavy-liquid separation was subsequently carried out using a lithium metatungstate solution with a density of 2.78 g cm^{-3}. After gentle stirring and sufficient settling time, the dense fraction containing conodont elements was collected, thoroughly rinsed with water, air-dried, and examined under a binocular microscope. All recovered conodont specimens are permanently housed at the Hubei Institute of Geosciences, Wuhan, China.

4 Results

Following laboratory processing, more than 1200 conodont specimens were recovered from 38 productive samples (Fig. 4). The majority of these specimens were obtained from the Longmenba section (approximately 500 specimens from 22 samples), the Huangping section (approximately 500 specimens from 12 samples), and the Tongmuyuan section (approximately 200 specimens from 4 samples). Taxonomic identification recognized 17 species belonging to four genera (Figs. 4–12), including *Hindeodus excavatus*, *H. typicalis*, *Jinogondolella prexuanhanensis*, *J. xuanhanensis*, *Clarkina dukouensis*, *C. asymmetrica*, *C. leveni*, *C. guangyuanensis*, *C. transcaucasica*, *C. liangshanensis*, *C. longicuspidata*, *C. wangi*, *C. subcarinata*, *C. changxingensis*, *C. orientalis*, *C. yini*, and *Iranognathus sosioensis*.

The conodont assemblages from the Longmenba (Figs. 5–9), Tongmuyuan (Figs. 10–11), and Huangping (Figs. 11–12) sections are moderately to well preserved and are dominated by *Clarkina* species in the Upper Permian strata and *Jinogondolella* species in the Guadalupian. These assemblages allow the recognition of several biostratigraphically significant intervals within the Dalong Formation and its adjacent strata (Fig. 4). In the Longmenba section, the lower part of the Dalong Formation yields abundant *Clarkina guangyuanensis*, *C. liangshanensis*, *C. transaucasica*, and *C. orientalis*. Upsection, the assemblage becomes dominated by *C. longicuspidata*, *C. wangi*, *C. subcarinata*, *C. changxingensis*, and *C. yini*, indicating a transition from the late Wuchiapingian to the Changhsingian. At the Huangping section, the conodont succession is broadly comparable. The lower Dalong Formation contains *C. orientalis* and rare *Iranognathus sosioensis*, suggesting an upper Wuchiapingian age, whereas the uppermost part of the formation yields *C. wangi*, *C. subcarinata*, and *C. changxingensis*, clearly indicating the Changhsingian. In the Tongmuyuan section, recovered conodonts include key taxa such as *C. transaucasica*, *C. changxingensis*, and *C. yini*, supporting a middle Wuchiapingian to Changhsingian age assignment.

Although direct conodont evidence is absent from the Chenjiawan and Longjingwan sections, distinctive lithological features and marker beds permit correlation with the biozones established in the conodont-bearing sections. This absence is most likely related to lithological and paleoenvironmental controls. The study area experienced rapid paleogeographic and environmental fluctuations during the Late Permian (Qiu et al., 2024), leading to pronounced lateral facies variability. Given the ecological sensitivity of conodont animals to seawater conditions, the lack of conodonts in these two sections may reflect unfavorable depositional settings. In particular, deeper-water intervals are commonly associated with siliceous sedimentation, which is less amenable to standard acetic acid processing and may hinder conodont recovery, whereas relatively shallow-water settings may not have supported conodont habitation.

Collectively, the 17 species identified from the three productive sections define a relatively continuous Wuchiapingian–Changhsingian conodont succession in the WHEC area, providing robust biostratigraphic control for the Upper Permian strata. Notably, the conodont-based biozones show a close stratigraphic correspondence with intervals of organic-rich shale within the Dalong Formation, underscoring the value of integrating high-resolution biostratigraphy with shale gas exploration.

5 Biostratigraphic zonation and chronostratigraphic discussion

5.1 *Jinogondolella xuanhanensis* Zone

The *Jinogondolella xuanhanensis* Zone is established in the uppermost Maokou and Gufeng formations of the Longmenba section, based on the first appearance of *J. xuanhanensis*. *Hindeodus* species and *J. prexuanhanensis* also occur within this zone, although the latter is restricted to its lowermost part (Fig. 4). *J. xuanhanensis* was first recognized from the Dukou section in Xuanhan County, eastern Sichuan Province (Mei et al., 1994a), and has since been widely reported from multiple sections in Guangxi, Guizhou, Hunan, and Jiangsu provinces of South China (Shen, 2023; Yuan et al., 2017, 2025). According to the recently standardized conodont biostratigraphic framework, the *Jinogondolella granti* Zone represents the terminal conodont zone of the Guadalupian (Shen et al., 2023; Yuan et al., 2025). *J. granti* is interpreted to have evolved from *J. xuanhanensis* through progressive flattening and fusion of the middle carina, enlargement of the posterior platform, and an increase in cusp size (Mei et al., 1994b). Although no specimens of *J. granti* were recovered in this study, this absence is consistent with previous observations that the *J. granti* Zone is missing or poorly developed in many sections across South China (Yuan et al., 2025). In the WHEC area, paleosol claystones, coal seams, and muddy siltstones are widely developed at the base of the Longtan Formation, suggesting the presence of a stratigraphic hiatus between the Gufeng and Longtan formations (Qiu et al., 2024; Zhang et al., 2025b).

The *Jinogondolella xuanhanensis* Zone is well represented in the uppermost Gufeng Formation at Longmenba and in other nearby sections (Zhang et al., 2025b), indicating that sedimentation persisted through much of the late Capitanian. In contrast, the overlying *J. granti* Zone is absent throughout the WHEC area, implying that deposition terminated shortly after the *J. xuanhanensis* interval. Notably, the uppermost part of the Gufeng Formation at Longmenba consists of thin-bedded siliceous rocks from which no conodonts were recovered (Fig. 4), rendering the thickness and precise stratigraphic position of the missing interval uncertain. Both lithostratigraphic (e.g., paleosol and coal seams) and biostratigraphic evidence therefore indicate a stratigraphic break above the *J. xuanhanensis* Zone. This hiatus is most plausi-

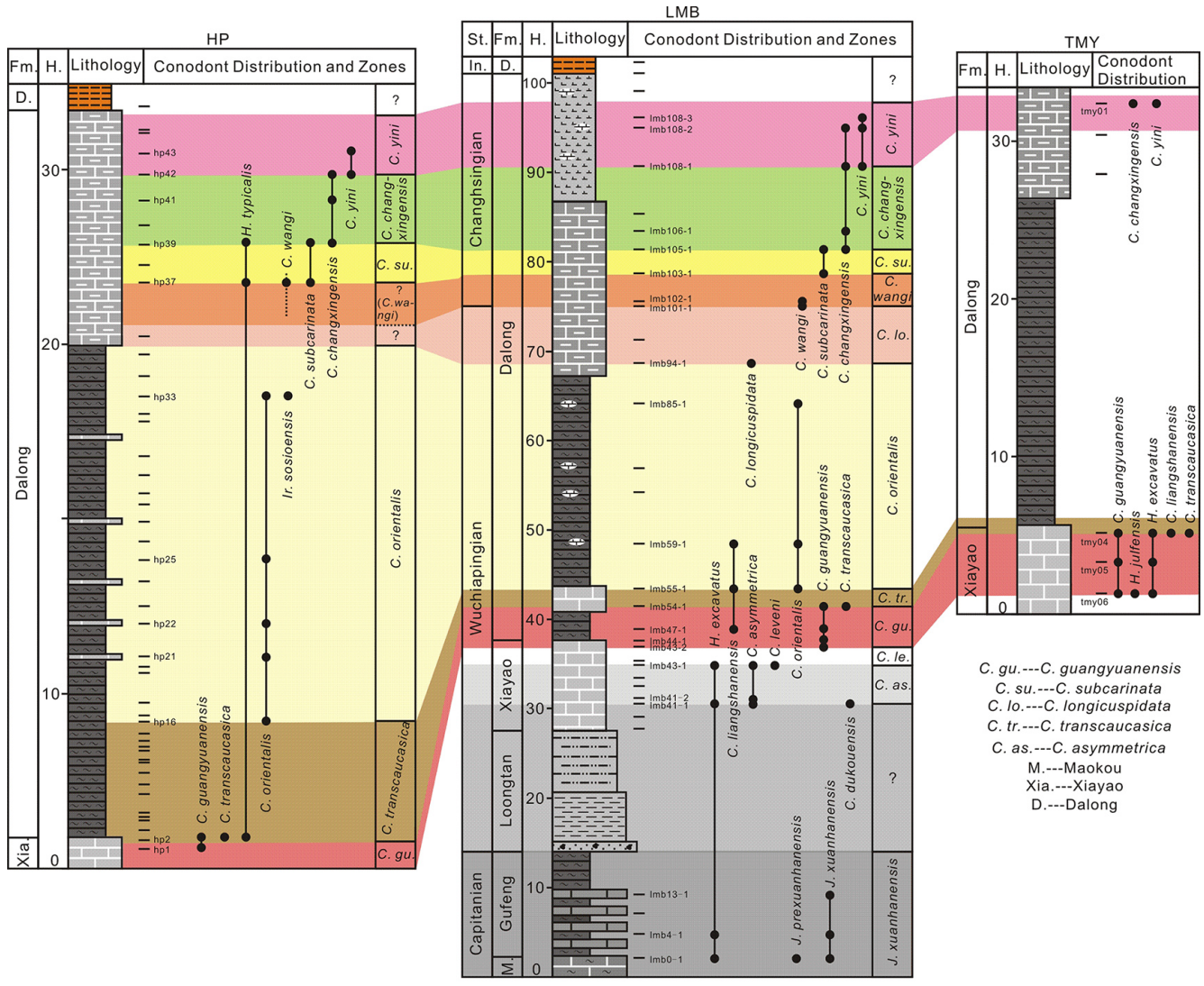

Figure 4. Stratigraphic range of conodont species recovered from the Huangping, Longmenba, and Tongmuyuan sections.

bly correlated with the Dongwu tectonic uplift and the associated sea level fall, which truncated the uppermost Guadalupian succession prior to deposition of the Longtan Formation (Hou et al., 2020; Qiu et al., 2024).

5.2 *Clarkina asymmetrica* Zone

The *Clarkina asymmetrica* Zone is recognized in the middle part of the Xiayao Formation at the Longmenba section. *Hindeodus excavatus* and *Clarkina dukouensis* also occur in the basal portion of this zone (Fig. 4). Both *C. asymmetrica* and *C. dukouensis* were originally described from the Dukou and Nanjiang sections of northeastern Sichuan, with *C. dukouensis* being interpreted to be the ancestral form of *C. asymmetrica* (Mei et al., 1994b). Near the Guadalupian–Lopingian boundary (GLB), species of the genus *Clarkina* progressively replaced *Jinogondolella* as the dominant conodont lineage, marking a major evolutionary turnover in Lopingian conodont faunas (Yuan et al., 2017). In 2006, the Global Stratotype Section and Point (GSSP) for the GLB was formally ratified at the Penglaitan section, where the first-appearance datum (FAD) of *Clarkina postbitteri postbitteri* defines the boundary (Jin et al., 2006a). Following submergence of the original Penglaitan section due to dam construction in 2020, a new GSSP candidate section and a Standard Auxiliary Boundary Stratotype (SABS) were established in the adjacent area (Shen et al., 2023). Detailed re-evaluation of these sections confirmed that the base of the Wuchiapingian Stage is defined by the FAD of *C. postbitteri* and proposed a well-resolved evolutionary lineage of *Jinogondolella granti* → *Clarkina postbitteri* → *C. dukouensis* (Shen et al., 2023). Accordingly, the *C. postbitteri* Zone is now regarded to be the lowermost conodont zone of the Lopingian (early

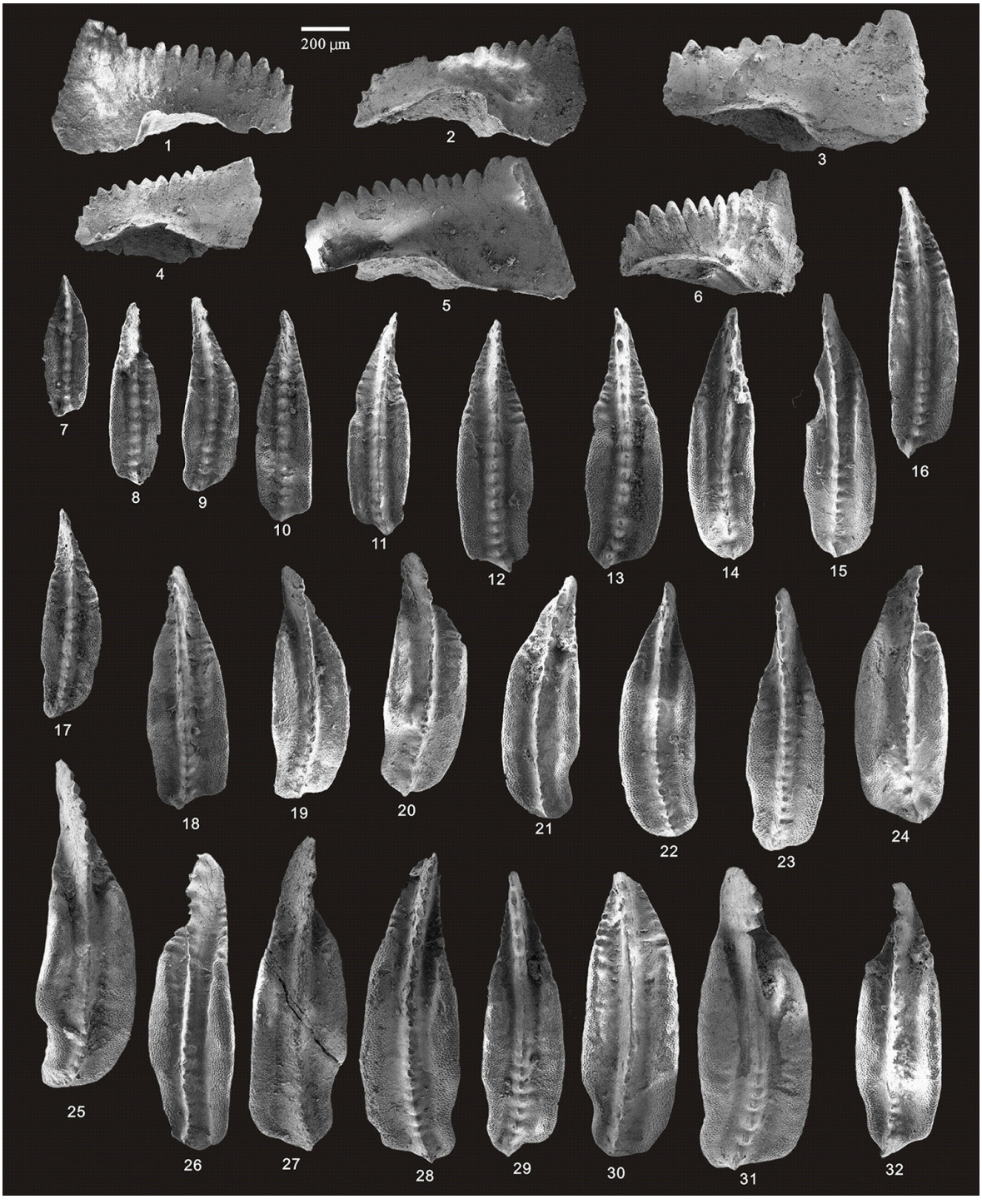

Figure 5. SEM photos of a selection of conodonts recovered from the Longmenba section. **(1–6)** *Hindeodus excavatus* (Behnken), HIG lmb01008–HIG lmb01013, from sample lmb0-1; **(7–8)** *Jinogondolella* sp., HIG lmb01017–HIG lmb01018, from sample lmb0-1; **(9–16)** *Jinogondolella prexuanhanensis* (Mei and Wardlaw), HIG lmb01019–HIG lmb01026, from sample lmb0-1; and **(17–32)** *Jinogondolella xuanhanensis* (Mei and Wardlaw), HIG lmb01033–HIG lmb01048, from sample lmb0-1.

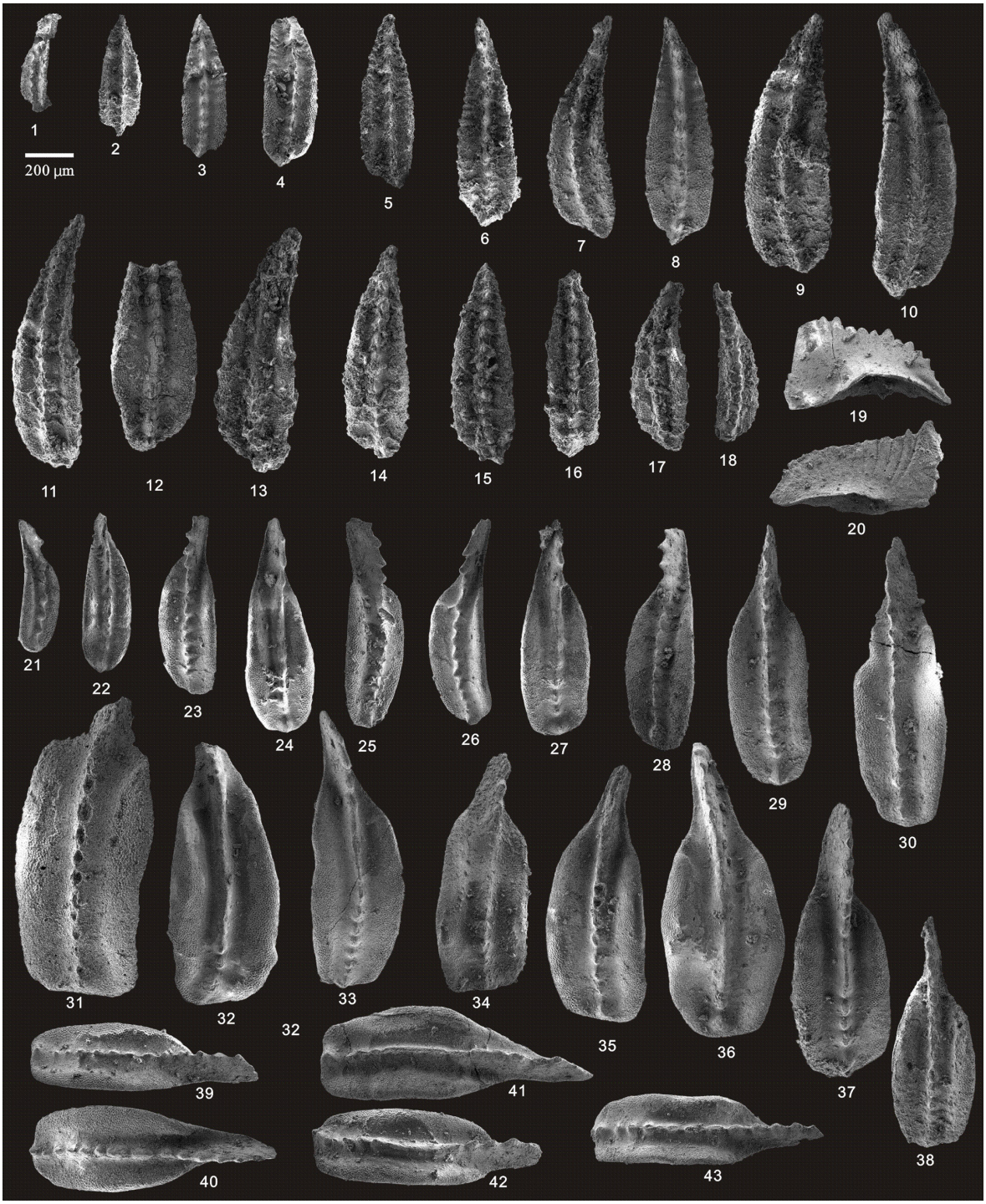

Figure 6. Continued. **(1–10)** *Jinogondolella xuanhanensis* (Mei and Wardlaw), HIG lmb04001–HIG lmb04010, from sample lmb4-1; **(11–18)** *Jinogondolella xuanhanensis* (Mei and Wardlaw), HIG lmb13001–HIG lmb13008, from sample lmb13-1; **(19–20)** *Hindeodus excavatus* (Behnken), HIG lmb41001–HIG lmb41002, from sample lmb41-1; **(21–30)** *Clarkina dukouensis* Mei and Wardlaw, HIG lmb41006–HIG lmb41015, from sample lmb41-1; **(31–39, 41)** *Clarkina asymmetrica* Mei and Wardlaw, HIG lmb41020–HIG lmb41028, HIG lmb41030, from sample lmb41-1; and **(40, 42–43)** *Clarkina* sp., HIG lmb41029, lmb41031–HIG lmb41032, from sample lmb41-1.

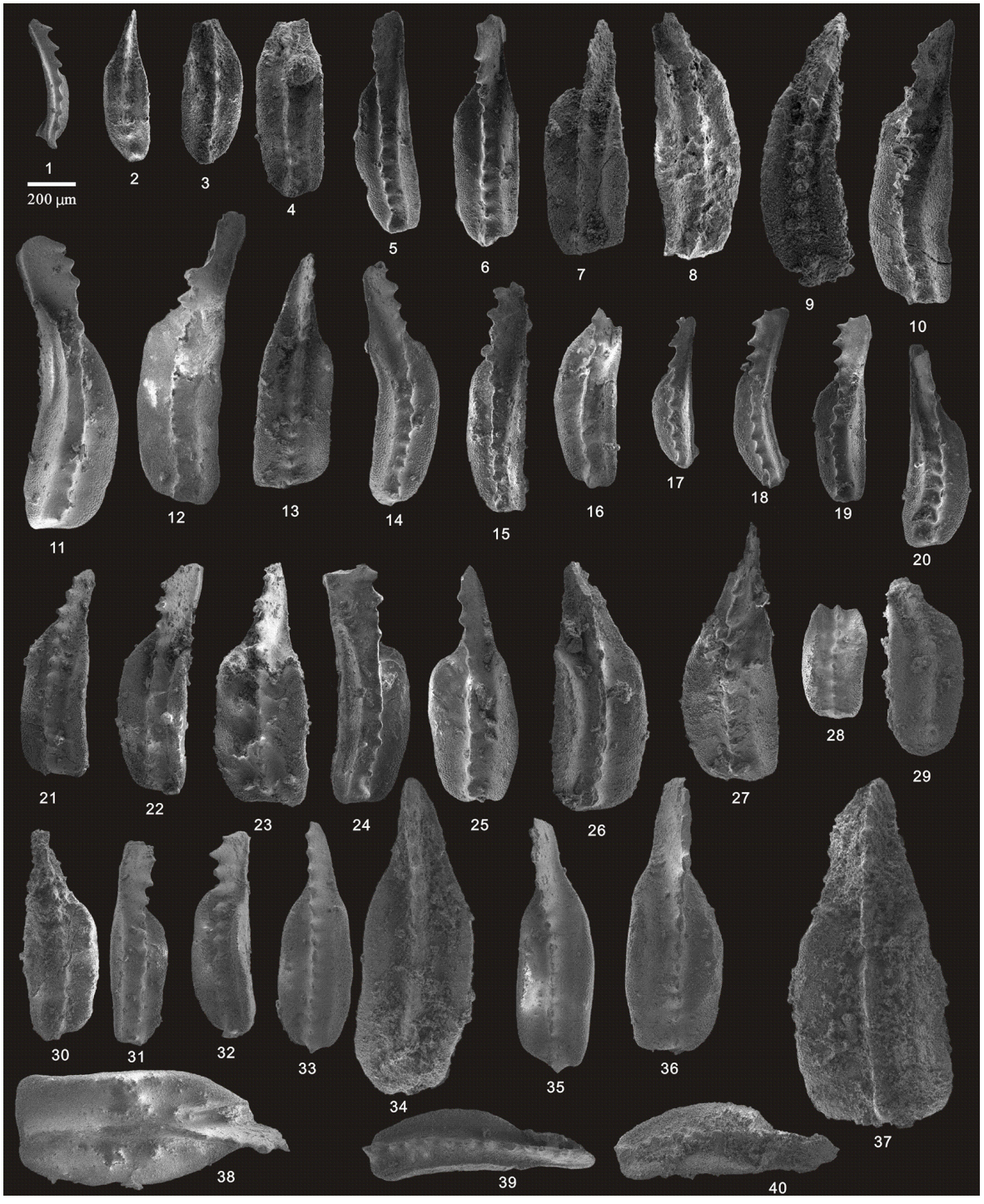

Figure 7. Continued. **(1–10)** *Clarkina asymmetrica* Mei and Wardlaw, HIG lmb41101–HIG lmb41110, from sample lmb41-2; **(11–16)** *Clarkina asymmetrica* Mei and Wardlaw, HIG lmb43001–HIG lmb43006, from sample lmb43-1; **(17–27)** *Clarkina leveni* (Kozur, Mostler, Pjatakova), HIG lmb43014–HIG lmb43024, from sample lmb43-1; **(28–38)** *Clarkina guangyuanensis* (Dai and Zhang), HIG lmb43101–HIG lmb43111, from sample lmb43-2; and **(39–40)** *Clarkina* sp., HIG lmb43112–HIG lmb43113, from sample lmb43-2.

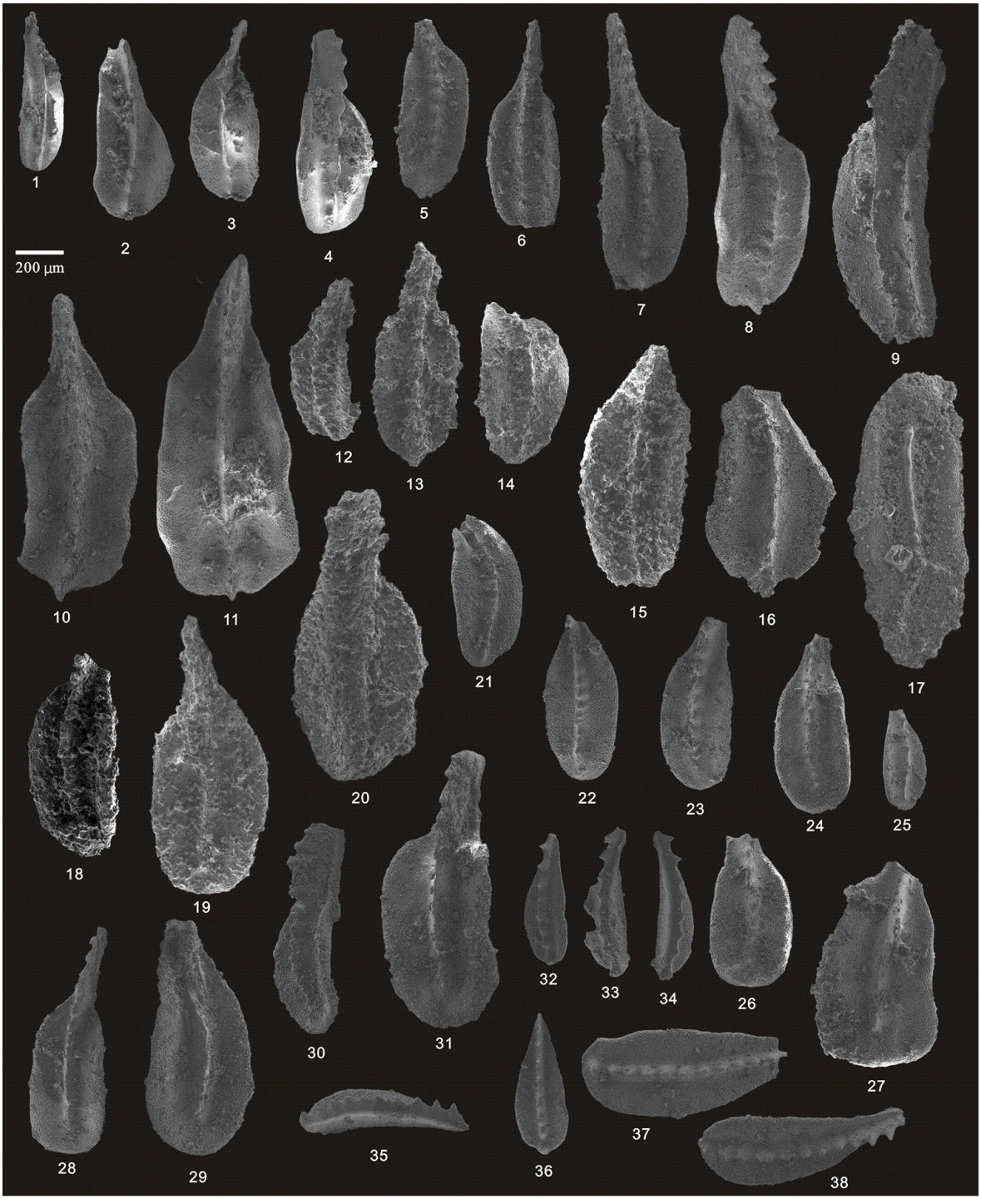

Figure 8. Continued. **(1–2)** *Clarkina liangshanensis* (Wang), HIG lmb47001–HIG lmb47002, from sample lmb47-1; **(3–4)** *Clarkina guangyuanensis* (Dai and Zhang), HIG lmb47003–HIG lmb13004, from sample lmb47-1; **(5–11)** *Clarkina guangyuanensis* (Dai and Zhang), HIG lmb54001–HIG lmb41007, from sample lmb54-1; **(12–17)** *Clarkina liangshanensis* (Wang), HIG lmb55005–HIG lmb55010, from sample lmb55-1; **(18–20)** *Clarkina orientalis* (Barskov and Koroleva), HIG lmb55001–HIG lmb55003, from sample lmb55-1; **(21–22)** *Clarkina liangshanensis* (Wang), HIG lmb59007–HIG lmb59008, from sample lmb59-1; **(23–27)** *Clarkina orientalis* (Barskov and Koroleva), HIG lmb59011–HIG lmb59015, from sample lmb59-1; **(28–31)** *Clarkina orientalis* (Barskov and Koroleva), HIG lmb59031–HIG lmb59035, from sample lmb59-1; and **(32–38)** *Clarkina longicuspidata* Mei and Wardlaw, HIG lmb94001–HIG lmb94007, from sample lmb94-1.

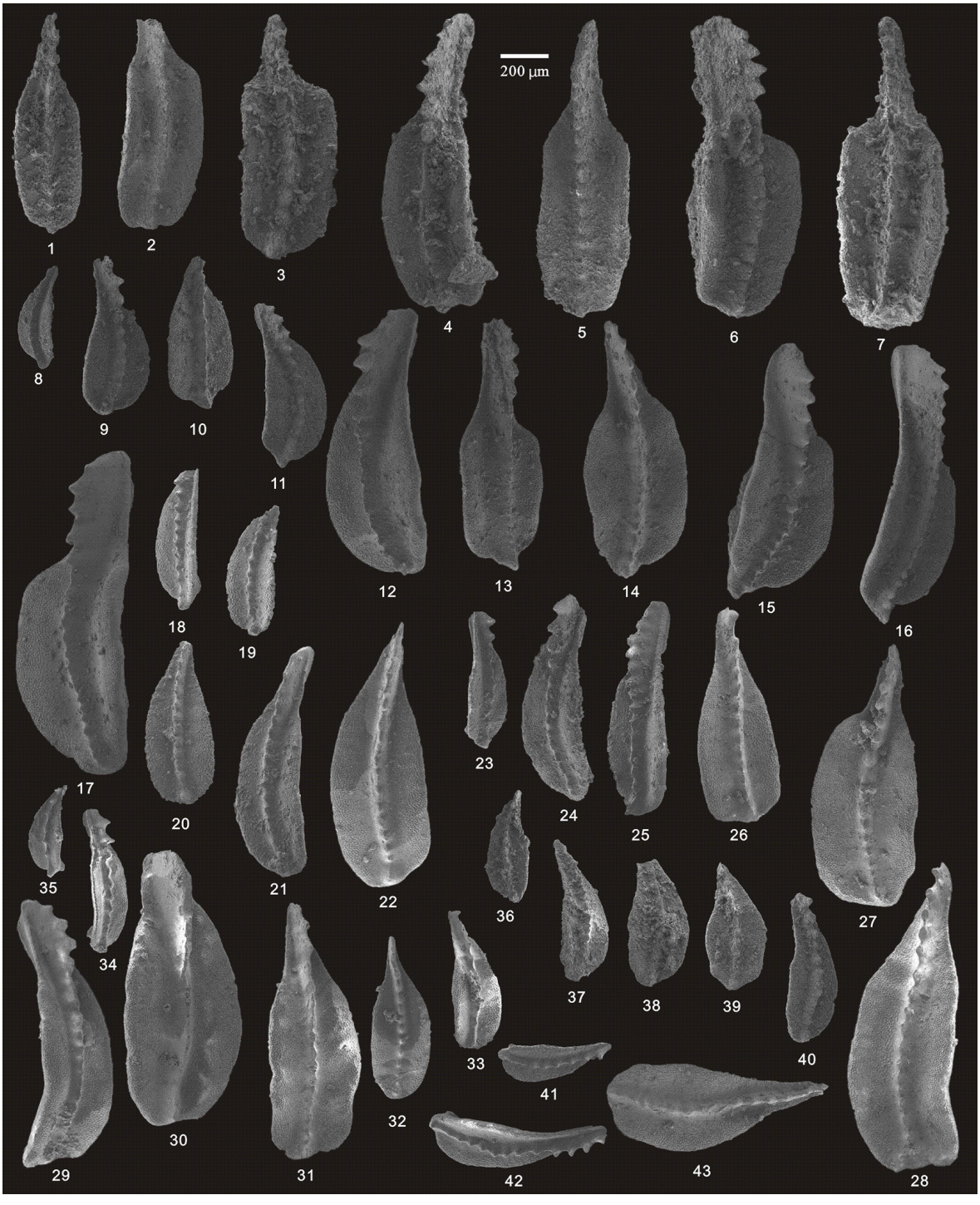

Figure 9. Continued. **(1–7)** *Clarkina transcaucasica* Gullo and Kozur, HIG lmb54017–HIG lmb54023, from sample lmb54-1; **(8–12)** *Clarkina wangi* (Zhang, 1987), HIG lmb101003–HIG lmb101007, from sample lmb101-1; **(13–16)** *Clarkina wangi* (Zhang, 1987), HIG lmb102001–HIG lmb102004, from sample lmb102-1; **(17)** *Clarkina wangi* transitional to *Clarkina subcarinata*, HIG lmb102005, from sample lmb102-1; **(18–22)** *Clarkina subcarinata* (Sweet), HIG lmb103001–HIG lmb103005, from sample lmb103-1; **(23–28)** *Clarkina subcarinata* (Sweet), HIG lmb105001–HIG lmb105006, from sample lmb105-1; **(29–35)** *Clarkina changxingensis* (Wang and Wang), HIG lmb105045–HIG lmb105051, from sample lmb105-1; **(36–40)** *Clarkina yini* Mei, HIG lmb108001–HIG lmb108005, from sample lmb108-1; and **(41–43)** *Clarkina yini* Mei, HIG lmb108301–HIG lmb108303, from sample lmb108-3.

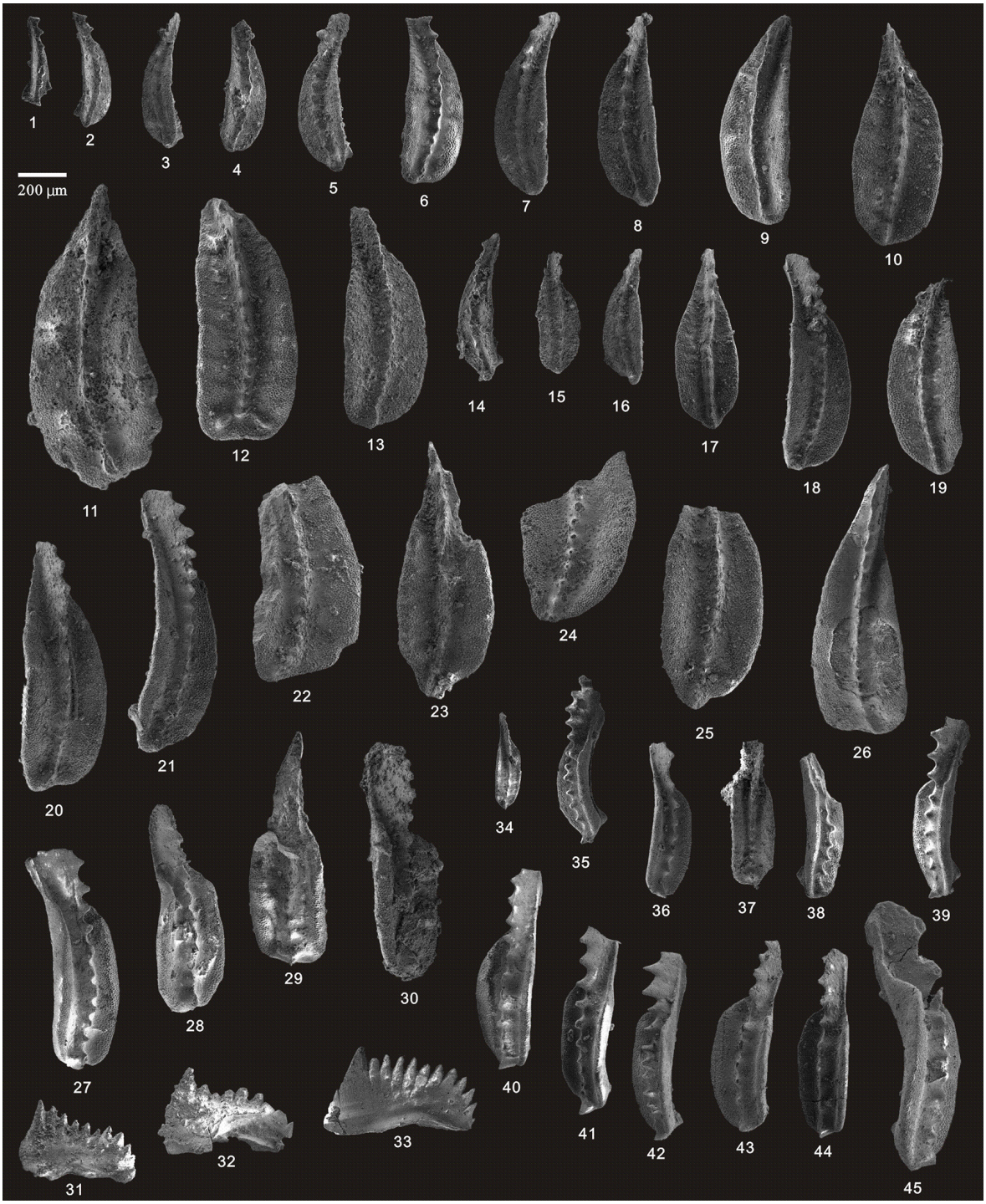

Figure 10. SEM photos of a selection of conodonts recovered from the Tongmuyuan section. **(1–13)** *Clarkina changxingensis* (Wang and Wang), HIG tmy01001–HIG tmy01013, from sample tmy-y01; **(14–25)** *Clarkina yini* Mei, HIG tmy01060–HIG tmy01071, from sample tmy-y01; **(26)** *Clarkina liangshanensis* (Wang), HIG tmy04001, from sample tmy-y04; **(27–30)** *Clarkina transcaucasica* Gullo and Kozur, HIG tmy04009–HIG tmy04012, from sample tmy-y04; **(31–33)** *Hindeodus excavatus* (Behnken), HIG tmy04002–HIG tmy04003, from sample tmy-y04; and **(34–45)** *Clarkina guangyuanensis* (Dai and Zhang), HIG tmy04020–HIG tmy04031, from sample tmy-y04.

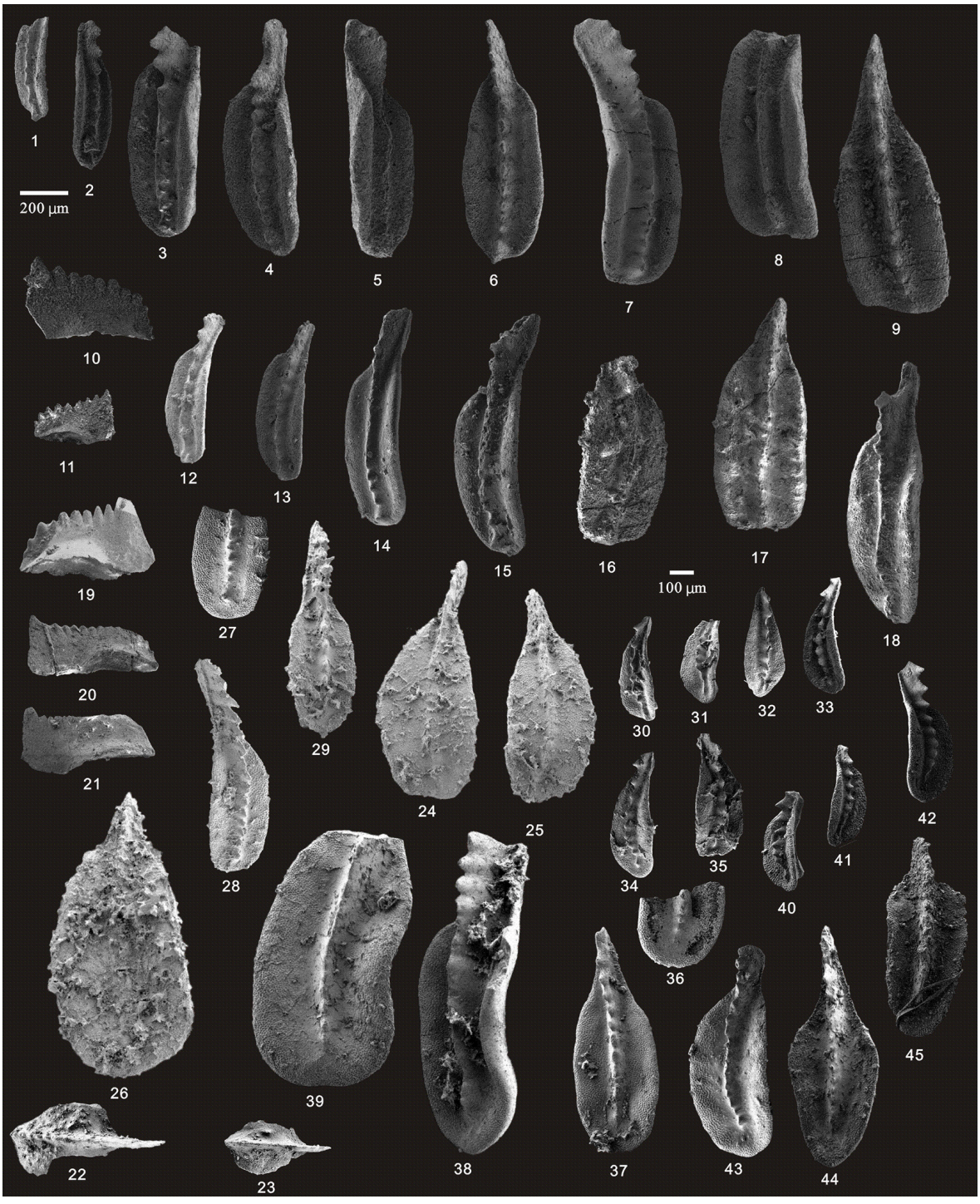

Figure 11. SEM photos of a selection of conodonts recovered from the Tongmuyuan and Huangping sections. **(1–9)** *Clarkina guangyuanensis* (Dai and Zhang), HIG tmy05001–HIG tmy05009, from sample tmy-y05; **(10–11)** *Hindeodus excavatus* (Behnken), HIG tmy05025–HIG tmy05026, from sample tmy-y05; **(12–17)** *Clarkina guangyuanensis* (Dai and Zhang), HIG tmy06002–HIG tmy06007, from sample tmy-y06; **(18)** *Clarkina* sp. (Dai and Zhang), HIG tmy06008, from sample tmy-y06; **(19)** *Hindeodus excavatus* (Behnken), HIG tmy06001, from sample tmy-y06; **(20–21)** *Hindeodus julfensis* (Sweet), HIG tmy06013–HIG tmy06014, from sample tmy-y06; **(22–23)** *Iranognathus sosioensis* Kozur and Mostler, HIG hp33001–HIG hp33002, from sample hp-33; **(24–29)** *Clarkina orientalis* (Barskov and Koroleva), HIG hp16001–HIG hp16005, from sample hp-16; **(30–39)** *Clarkina orientalis* (Barskov and Koroleva), HIG hp21001–HIG hp21010, from sample hp-21; **(40–45)** *Clarkina orientalis* (Barskov and Koroleva), HIG hp33001–HIG hp33006, from sample hp-33.

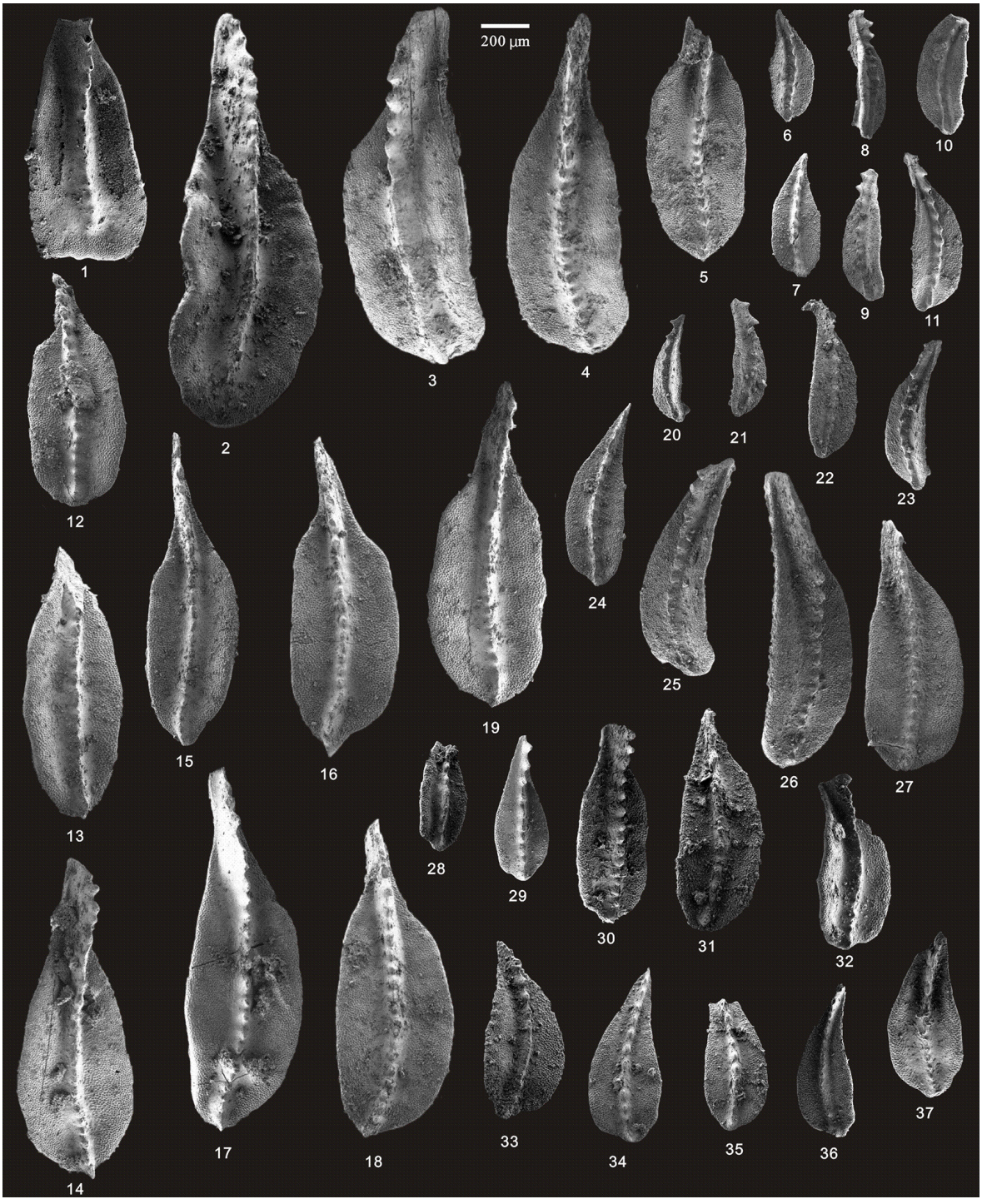

Figure 12. SEM photos of a selection of conodonts recovered from the Huangping section. **(1–2)** *Clarkina orientalis* (Barskov and Koroleva), HIG hp33007–HIG hp33008, from sample hp-33; **(3–7)** *Clarkina subcarinata* (Sweet), HIG hp39004–HIG hp39008, from sample hp-39; **(8–19)** *Clarkina changxingensis* (Wang and Wang), HIG hp39085–HIG hp39096, from sample hp-39; **(20–27)** *Clarkina changxingensis* (Wang and Wang), HIG hp41001–HIG hp41008, from sample hp-41; **(28–32)** *Clarkina yini* Mei, HIG hp42001–HIG hp42005, from sample hp-42; **(33–37)** *Clarkina yini* Mei, HIG hp43001–HIG hp43005, from sample hp-43.

Wuchiapingian), followed upward by the *C. dukouensis* and *C. asymmetrica* zones.

Owing to a widespread regional regression near the end of the Guadalupian, the *C. dukouensis* Zone commonly represents the earliest preserved Wuchiapingian conodont interval in many sections across South China (Yuan et al., 2017, 2019). Morphologically, *C. asymmetrica* can be distinguished from *C. dukouensis* by the asymmetrical narrowing of the anterior platform, more extensively fused denticles along the middle carina, and the presence of a small gap between the cusp and the posteriormost denticle (Mei et al., 1994b; Yuan et al., 2017). However, gerontic specimens of *C. dukouensis* may exhibit increased carinal fusion, resulting in morphologies that closely resemble *C. asymmetrica* (Yuan et al., 2017). In the Longmenba section, both *C. asymmetrica* and *C. dukouensis* were recovered from the lowermost part of the *C. asymmetrica* Zone (Fig. 4). The *C. dukouensis* specimens display partially fused carina, supporting a transitional morphological relationship between the two species and indicating that the lower portion of the *C. asymmetrica* Zone represents an evolutionary continuum rather than an abrupt faunal replacement. Stratigraphically, the overlying Longtan and Xiayao formations record a renewed transgressive phase following the Guadalupian–Lopingian regression, consistently with regional sea level rise along the WHEC margin.

5.3 *Clarkina leveni* Zone

The *Clarkina leveni* Zone is recognized in the upper part of the Xiayao Formation at the Longmenba section (Fig. 4). Associated conodont taxa include *Hindeodus excavatus* and *Clarkina asymmetrica*. *C. leveni* was originally described from Archura in Transcaucasia, and subsequent reports from South China are rare and geographically restricted. Within South China, this species has been documented only from limited stratigraphic horizons, typically represented by one or two productive samples, in Guizhou, Sichuan, Hubei, Hunan, and Guangxi provinces (Kozur, 1975; Wang and Dong, 1991; Mei et al., 1994b, c; Zhang et al., 2007; Bagherpour et al., 2018a). Although Shen and Mei (2010) reported *C. leveni* from Iranian tectonic blocks, a subsequent re-evaluation of the Abadeh section in central Iran yielded only a tentative occurrence of this species (Yuan et al., 2025).

Quantitative biochronological analyses further indicate that the *Clarkina leveni* Zone is either poorly developed or extremely short-lived (Yuan et al., 2019). Consistently with this interpretation, *C. leveni* was recovered together with *C. asymmetrica* from only a single sample in the Longmenba section (Fig. 4), supporting the inference that this zone represents a very brief stratigraphic interval. Regionally, the *C. leveni* Zone corresponds to the terminal phase of the Wuchiapingian regression (Hou et al., 2020). In contrast, the overlying Dalong Formation and the upper part of the Xiayao Formation record a subsequent deepening trend, characterized by the development of organic-rich siliceous shales in the WHEC area. The sharp facies transition across this interval, combined with the limited stratigraphic distribution of *C. leveni*, suggests that the brevity of the *C. leveni* Zone reflects both a short-lived evolutionary episode within the *Clarkina* lineage and a condensed depositional regime associated with the transition from regressive to transgressive conditions along the WHEC margin.

5.4 *Clarkina guangyuanensis* Zone

The *Clarkina guangyuanensis* Zone is recognized in the Longmenba, Huangping, and Tongmuyuan sections, although its precise stratigraphic position shows minor variation among these localities (Fig. 4). *C. guangyuanensis* was originally described from the Wuchiaping Formation in Sichuan Province (Li et al., 1989), and its distribution has since been documented widely across South China (Yuan et al., 2017; Bagherpour et al., 2018a; Zhang et al., 2021). Additional occurrences from the southern Lhasa Terrane and several tectonic blocks in Iran further expand the paleogeographic range of this species, indicating its broad distribution along the Paleo-Tethyan realm during the Wuchiapingian (Shen and Mei, 2010; Wu et al., 2021; Yuan et al., 2019, 2025). Morphologically, *C. guangyuanensis* is characterized by a large cusp that is markedly higher than the posterior denticles, with a small but distinct gap between the cusp and the first posterior denticle. Compared with *C. leveni*, *C. guangyuanensis* exhibits a wider and longer platform, a sharper anterior margin, and a more pronounced gap between the cusp and posterior denticle (Yuan et al., 2017).

In the Longmenba and Huangping sections, the *C. guangyuanensis* Zone occurs near the top of the Xiayao Formation, where *C. guangyuanensis* is the sole conodont taxon recovered (Fig. 4). In the Tongmuyuan section, *C. guangyuanensis* is likewise present, although the apparent base of the zone occurs slightly lower stratigraphically. At this locality, *Hindeodus excavatus* and *H. julfensis* co-occur with *C. guangyuanensis*. Because the Xiayao Formation is not fully exposed in the Tongmuyuan section, the precise position of the base of the zone cannot be confidently determined. Nevertheless, the consistent occurrence of *C. guangyuanensis*, either alone or in association with *Hindeodus* species, supports assignment of this interval to the early–middle Wuchiapingian (Yuan et al., 2017; Zhang et al., 2024).

In addition to *Clarkina guangyuanensis*, another taxon of stratigraphic significance, *C. liangshanensis*, is recovered from the lowermost Dalong Formation in the Longmenba section and from the uppermost limestone of the Xiayao Formation in the Tongmuyuan section. In Tongmuyuan, its co-occurrence with *C. transcaucasica* suggests that *C. liangshanensis* may have appeared slightly earlier there than in Longmenba. However, incomplete exposure of the lower Xiayao Formation precludes a precise assessment of its true first appearance in this section (Fig. 4). *C. liangshanensis* was first described from the Liangshan area of Hanzhong

City, Shaanxi Province (Wang, 1978), and has subsequently been reported from South China, the southern Lhasa Terrane, and Iran, indicating a relatively long stratigraphic range (Yuan et al., 2014, 2017, 2025; Wu et al., 2021; Zhang et al., 2024). Morphologically, *C. liangshanensis* differs from *C. guangyuanensis* in that it possesses a very small or inconspicuous cusp and a relatively wide posterior platform margin. Owing to these features, *C. liangshanensis* has been regarded to be the ancestral form of *C. orientalis* (Yuan et al., 2014).

Although the *Clarkina liangshanensis* Zone is commonly placed immediately above the *C. guangyuanensis* Zone in standard Wuchiapingian conodont zonations, recent studies suggest that the first appearance of *C. liangshanensis* may be diachronous and taxonomically complex, particularly in relation to coeval species such as *C. guangyuanensis* and *C. transcaucasica* (Zhang et al., 2024; Yuan et al., 2025). These complexities likely reflect both morphological convergence within the *Clarkina* lineage and facies-dependent controls on species distribution. In the WHEC area, *C. guangyuanensis* consistently appears below *C. liangshanensis* across all productive sections. Accordingly, the *C. guangyuanensis* Zone is retained here as a practical and stratigraphically robust biostratigraphic unit for correlating the upper Xiayao Formation and the onset of Dalong Formation deposition.

5.5 *Clarkina transcaucasica* Zone

The *Clarkina transcaucasica* Zone is recognized in the Longmenba, Huangping, and Tongmuyuan sections (Fig. 4). *C. transacucasica* was first described from western Sicily, Italy, originally as a subspecies of *C. orientalis* (Gullo and Kozur, 1992). It is morphologically distinguished by a very broad platform, a small but erect cusp, a squared posterior termination, and the general absence of a gap between the cusp and the first posterior denticle (Yuan et al., 2017), features that allow reliable separation from co-occurring *Clarkina* species.

In the Huangping and Tongmuyuan sections, the first occurrence of *Clarkina transcaucasica* is recorded from the uppermost limestone beds of the Xiayao Formation. In contrast, at Longmenba, *C. transcaucasica* occurs above an approximately 4 m thick basal limestone unit that directly overlies the black siliceous shales of the Dalong Formation (Fig. 4). This apparent discrepancy in stratigraphic position among the studied sections is best explained by local lithofacies variations and subtle diachroneity in conodont distribution rather than by major stratigraphic omission. From a regional perspective, the first appearance of *C. transcaucasica* broadly coincides with the transition from the regressive, relatively shallow-water conditions of the early Wuchiapingian to a subsequent deepening phase that culminated in the widespread deposition of organic-rich siliceous shales of the Dalong Formation. In all three sections, strata yielding *C. transcaucasica* occur immediately below, or locally within, the basal part of the Dalong Formation. Consequently, the *C. transcaucasica* Zone provides a robust biostratigraphic marker for identifying the onset of deep-water sedimentation and associated environmental reorganization in the WHEC area.

5.6 *Clarkina orientalis* Zone

The *Clarkina orientalis* Zone is recognized in the Huangping and Longmenba sections, where the first occurrence of *C. orientalis* is located close to the base of the Dalong Formation (Fig. 4). In the Longmenba section, this taxon appears immediately above strata yielding *C. transcaucasica*, a stratigraphic relationship that is fully consistent with the established late Wuchiapingian conodont zonal succession in South China (Yuan et al., 2017). Morphologically, *C. orientalis* is characterized by a broad, subrectangular platform, a centrally positioned cusp, and a weakly ornamented posterior margin. These features distinguish it from *C. liangshanensis* and support its interpretation as a more derived taxon within the *Clarkina* evolutionary lineage (Yuan et al., 2014, 2017, 2025).

In the Tongmuyuan section, however, the *Clarkina orientalis* Zone could not be identified (Fig. 4). This absence is most plausibly attributed to lithological and methodological limitations rather than to a true biological or stratigraphic gap. The acetic-acid maceration method employed in this study is inherently less effective for siliceous and argillaceous lithologies, and the lower Dalong Formation at Tongmuyuan lacks limestone interbeds or carbonate nodules that would facilitate conodont recovery. As a result, the non-occurrence of *C. orientalis* at this locality is best interpreted as a facies-controlled sampling bias.

Despite its uneven distribution among the studied sections, the consistent and well-constrained occurrence of *C. orientalis* in the Huangping and Longmenba sections enables high-resolution biostratigraphic subdivision of the lower Dalong Formation. Regionally, *C. orientalis* is a key marker taxon for the late Wuchiapingian and has been widely documented across South China, the Lhasa Terrane, and several peri-Gondwanan regions (Yuan et al., 2014, 2017, 2019, 2025; Bagherpour et al., 2018a). Within the WHEC area, the lowest occurrence of *C. orientalis* falls within facies recording the early stage of deep-water sedimentation, although a thin limestone unit still underlies this horizon in the Longmenba section. This relationship indicates that the *C. orientalis* Zone postdates the initial basin deepening and instead represents a subsequent stage within an already established deep-water regime. Accordingly, the *C. orientalis* Zone provides a reliable biostratigraphic marker for correlating and subdividing the lower deep-water portion of the Dalong Formation (Fig. 4).

5.7 *Clarkina longicuspidata* Zone

The *Clarkina longicuspidata* Zone is recognized from a muddy-limestone interval in the middle part of the Dalong Formation in the Longmenba section (Fig. 4). No other conodont taxa were recovered from this interval. *C. longicuspidata* is characterized by an elongated cusp, a narrow anterior platform, and moderately fused posterior denticles, which distinguish it from coeval taxa such as *C. wangi* and *C. subcarinata* (Yuan et al., 2014). The species was originally described from northeastern Sichuan Province, but subsequent reports remain relatively scarce (Mei et al., 1994a; Nafi et al., 2006; Yuan et al., 2014; Zhang et al., 2021). Although no formal *C. longicuspidata* Zone was erected there, Nafi et al. (2006) documented its occurrence in the Ganxi section of western Hubei, likely reflecting its limited stratigraphic range. Despite extensive sampling, *C. longicuspidata* has not been recovered from the well-studied Shangsi section (Yuan et al., 2019). Kozur (2005) tentatively reported a possible occurrence in the Abadeh section in Iran; however, the lack of illustration and subsequent reassessment failed to confirm this identification (Yuan et al., 2025). Accordingly, the interval assigned to the *C. longicuspidata* Zone by Kozur (2005) is now considered to more plausibly correspond to the uppermost part of the *C. orientalis* Zone (Yuan et al., 2025).

At Longmenba, the first appearance of *Clarkina longicuspidata* occurs immediately above the thin-bedded siliceous rocks that typify the preceding deep-water, silica-rich facies (Fig. 4). The coincident transition to muddy-limestone deposition marks a relative shallowing of the depositional environment (Xu et al., 2025). This lithofacies shift, characterized by reduced silica influx and increased carbonate sedimentation, indicates that the *C. longicuspidata* Zone represents the early stage of a deep-to-shallow water transition rather than continued deepening.

Although the Longmenba section preserves the most complete expression of this zone, the known ecological distribution of *Clarkina longicuspidata* suggests that its true evolutionary first appearance may lie stratigraphically below the lowest recovered specimens. The siliceous beds underlying the zone yield only rare and poorly preserved conodont elements, precluding reliable species-level identification. Consequently, the base of the *C. longicuspidata* Zone at Longmenba represents the lowest stratigraphic level at which the species can be confidently recognized and is therefore likely to be truncated by facies-dependent preservational bias of the scattered but environmentally coherent distribution of *C. longicuspidata* in South China. The species has been reported from deeper-water siliceous mudstone in both the Ganxi section of western Hubei and the Longwangpo section of northwestern Guangxi (Nafi et al., 2006; Zhang et al., 2021), yet it remains absent from numerous coeval carbonate-dominated sections. Such a pattern implies a short stratigraphic range coupled with strong facies control on preservation (Mei et al., 1994a; Nafi et al., 2006; Yuan et al., 2014, 2019; Zhang et al., 2021). Its rarity, brief temporal duration, and selective preservation help explain the difficulty in establishing a well-defined *C. longicuspidata* Zone elsewhere. Despite these limitations, the Longmenba section provides a rare and stratigraphically reliable record of this biohorizon, significantly improving the high-resolution biostratigraphic subdivision of the Dalong Formation in the WHEC area.

5.8 *Clarkina wangi* Zone

The *Clarkina wangi* Zone is recognized in the Longmenba section (Fig. 4). In the Huangping section, *C. wangi* also occurs in the upper part of the Dalong Formation, where it co-occurs with *C. subcarinata*. *C. wangi* is characterized by strongly fused denticles and a reclined cusp that is approximately equal in height to the adjacent denticles, giving the element a distinctive wall-like outline. The carina typically extends beyond the posterior platform margin, resulting in a pointed posterior termination (Mei et al., 2004; Yuan et al, 2014). This species was originally described as a subspecies, *Clarkina* (*Neogondolella*) *subcarinata elongata* (Wang and Wang, 1981a, b), and was later formally elevated to species rank as *C. wangi* based on material from the Changxing area of Zhejiang Province (Zhang, 1987).

Morphologically, *Clarkina wangi* occupies an intermediate yet diagnostically distinct position within the evolutionary lineage bounded by *C. longicuspidata* and *C. subcarinata* (Mei et al., 2004; Yuan et al., 2014). It differs from its descendant *C. subcarinata* in possessing a higher and more strongly fused carina, a shorter and more erect cusp, and a shorter, wider platform. In contrast, its inferred ancestor *C. longicuspidata* displays a distinct gap between the cusp and the first posterior denticle and a narrower platform, reflecting an earlier stage of posterior platform integration.

The GSSP for the base of the Wuchiapingian Stage was ratified in 2006 at the Meishan D section, Changxing County, Zhejiang Province (Jin et al., 2006b), where the first appearance datum (FAD) of *Clarkina wangi* was adopted as the primary marker for the Wuchiapingian–Changhsingian boundary. The recognition of *C. wangi* in both the Longmenba and Huangping sections therefore provides a robust linkage to the global conodont zonation and serves as a reliable calibration horizon for high-resolution intra-basinal correlation within the Dalong Formation in the study area.

5.9 *Clarkina subcarinata* Zone

The *Clarkina subcarinata* Zone is recognized in both the Huangping and Longmenba sections based on the first occurrence of this species (Fig. 4). In the Huangping section, *C. subcarinata* co-occurs with *Hindeodus typicalis*, suggesting a slightly shallower, though still offshore, depositional setting relative to the underlying intervals. Previous studies from across South China indicate that the *C. subcar-*

inata Zone represents a temporally short interval, comparable to the underlying *C. wangi* Zone, and reflects rapid conodont evolutionary turnover near the Wuchiapingian–Changhsingian transition (Henderson, 2018; Metcalfe and Crowley, 2020). The present observations are consistent with this pattern: *C. subcarinata*-bearing intervals in the studied sections are thin, occupy comparable stratigraphic positions, and show similar thicknesses across the area (Fig. 4), collectively indicating a broadly synchronous appearance and a brief stratigraphic range.

Clarkina subcarinata is readily distinguished within the Changhsingian conodont succession by its characteristic platform morphology. The species possesses a long, symmetrical platform with a bluntly to squarely rounded posterior termination; a small erect cusp that is equal to or slightly higher than the posterior denticles; and a low, partially fused carina that maintains a relatively uniform height and does not extend beyond the posterior platform margin (Yuan et al., 2014). Compared with its successor (*C. changxingensis*), *C. subcarinata* exhibits a less pronounced or absent gap between the cusp and the posteriormost denticle, a more squared posterior platform termination, and a subtler cusp, together providing a reliable basis for biostratigraphic discrimination (Yuan et al., 2014).

Regionally, the occurrence of *C. subcarinata* corresponds to a phase of relatively stable deep-water deposition within the WHEC area following the water depth fluctuations recorded during the *C. orientalis* and *C. longicuspidata* intervals (Fig. 4). Accordingly, the *C. subcarinata* Zone serves as an important stratigraphic marker for correlating the upper Dalong Formation and for constraining shale-gas-bearing intervals within Upper Permian successions of the study area.

5.10 *Clarkina changxingensis* Zone

The *Clarkina changxingensis* Zone is recognized in both the Huangping and Longmenba sections based on the first appearance of this species (Fig. 4). As a widely accepted indicator of latest Wuchiapingian to earliest Changhsingian deposition, the occurrence of *C. changxingensis* provides an important biostratigraphic marker for refining the upper Dalong Formation in the study area. In the Huangping section, *C. changxingensis* co-occurs with *Hindeodus typicalis*, a taxon commonly present in offshore to outer-shelf facies of the Lopingian but lacking diagnostic zonal significance. In the Tongmuyuan section, *C. changxingensis* occurs together with *C. yini* within muddy limestone of the Dalong Formation (sample tmy01). Because *C. yini* defines the succeeding biozone, this association indicates a condensed or mixed conodont assemblage in this interval. As a result, the *C. changxingensis* Zone cannot be formally established at Tongmuyuan. Nevertheless, the consistent and stratigraphically coherent occurrence of *C. changxingensis* in the Huangping and Longmenba sections demonstrates that this species has a regionally stable distribution within the upper Dalong Formation.

Clarkina changxingensis exhibits a distinctive yet internally variable platform morphology, reflecting its prolonged evolutionary history during the Changhsingian. Although the species displays considerable intraspecific variation, its morphological development follows a recognizable evolutionary trajectory that provides a robust basis for taxonomic identification and stratigraphic application (Yuan et al., 2014). The species is characterized by an elongate platform with its maximum width near the middle, a variable posterior termination, and an erect to reclined cusp that is equal to or slightly higher and larger than the posterior denticles. A gap is typically present between the cusp and the posteriormost denticle or between the cusp and the second posteriormost denticle when fusion occurs. At the Meishan section, *C. changxingensis* spans a duration exceeding 1 Myr, encompassing approximately half of the Changhsingian, and three successive morphological stages have been recognized (Yuan et al., 2014): (1) an early stage with an inconspicuous gap and a rounded posterior platform end; (2) an intermediate stage characterized by a pronounced gap and an extended posterior termination; and (3) an advanced stage marked either by an extended posterior end and a reduced erect cusp resembling *C. yini* or by a large cusp, narrow platform, and moderately developed furrows approaching the morphology of *C. meishanensis*. Regionally, the appearance of *Clarkina changxingensis* corresponds to continued deep-water, low-energy sedimentation throughout the upper Dalong Formation, consistently with the broader evolutionary pattern of conodont assemblages during the middle Changhsingian in South China. Consequently, the *C. changxingensis* Zone serves as a key reference interval for correlating middle Changhsingian strata across the WHEC area and for refining the stratigraphic framework relevant to shale-gas-bearing Upper Permian successions.

5.11 *Clarkina yini* Zone

The *Clarkina yini* Zone is recognized in the Huangping and Longmenba sections based on the first appearance of this species (Fig. 4). The occurrence of *C. yini* in the Tongmuyuan section further suggests that this zone is also likely to be present there; however, its formal establishment is currently precluded by the limited number of available samples. This pattern indicates that the stratigraphic distribution of *C. yini* within the study area may be broader than presently documented and that higher-resolution sampling has the potential to refine the biostratigraphic framework of the Tongmuyuan succession. In addition, the uppermost Dalong Formation in both the Huangping and Longmenba sections is dominated by muddy limestone and mudstone lithologies, which are generally less responsive to standard acetic-acid processing. Reduced recovery efficiency of conodont elements in these intervals may therefore partly account for the apparently sparse record of *C. yini*. Nevertheless, previous

studies from western Hubei have demonstrated that a complete and continuous conodont succession can be established across this interval in both deep-water and shallow-water settings (Lyu et al., 2019; Yang et al., 2019; Du et al., 2025). These results support the expectation that *C. yini* should have a stable and traceable presence in the study area once sampling density and processing resolution are improved.

Morphologically, *Clarkina yini* is characterized by a bluntly rounded posterior termination and a distinctive spout-like posterior platform extension, formed by two shallow indentations on either side of the posterior margin (Yuan et al., 2014). This configuration gives the impression that the carina, or the posteriorly reclined cusp, extends beyond the posterior edge of the platform. The denticles are generally uniform in height, and a pronounced concavity is typically developed between the cusp and the posteriormost denticle. Additional diagnostic features include a flattened posterior platform surface and a narrow brim immediately posterior to the cusp. In oral view, *C. yini* may superficially resemble *C. wangi*; however, it can be readily distinguished by its shorter and less fused carina, together with its more strongly developed posterior platform extension.

Regionally, the first appearance of *C. yini* marks a critical evolutionary and stratigraphic turning point near the top of the Dalong Formation, corresponding to the late Changhsingian interval immediately preceding the end-Permian mass extinction (Yuan et al., 2014; Lyu et al., 2019). Owing to its short temporal range, *C. yini* is regarded to be a high-resolution biostratigraphic marker within Upper Permian successions of South China (Yuan et al., 2014; Henderson, 2018). Its recognition in the studied sections therefore provides an important chronostratigraphic constraint on the terminal Permian depositional history of the WHEC area.

6 Discussion

6.1 Conodont biostratigraphy and the Wuchiapingian–Changhsingian Boundary in the WHEC area

The conodont assemblages recovered from the Longmenba, Huangping, and Tongmuyuan sections collectively document a near-continuous Lopingian record spanning the critical Wuchiapingian–Changhsingian transition (Fig. 4). These assemblages record a successive appearance of key taxa, including *Jinogondolella xuanhanensis*, *Clarkina asymmetrica*, *C. leveni*, *C. guangyuanensis*, *C. transcaucasica*, *C. orientalis*, *C. longicuspidata*, *C. wangi*, *C. changxingensis*, and *C. yini*. Together, these species define a coherent conodont zonal sequence that closely corresponds to the GSSP-calibrated framework established at Meishan and other well-studied sections in South China (Yuan et al., 2014, 2017, 2019).

Notably, *Clarkina dukouensis*, a taxon commonly regarded to be an index species for the lower Wuchiapingian (Yuan et al., 2014), is present in the study area. However, its observed first occurrence coincides with the base of the overlying *C. asymmetrica* Zone. This pattern suggests that the true first appearance of *C. dukouensis* may lie at lower stratigraphic levels in the Longmenba section. Its apparent absence from the lower parts of the studied successions likely reflects a combination of local stratigraphic condensation or minor hiatuses near the base of the Longtan Formation, as well as limited preservation potential within the thick siliciclastic-dominated intervals. When integrated with the regional conodont framework, these observations indicate that the WHEC area preserves a broadly continuous marine succession across the Guadalupian–Lopingian transition, with the exception of the *J. granti*, *C. postbitteri*, and *C. dukouensis* zones that are typically developed in more complete South China successions.

As the terminal stage of the Permian, the Changhsingian records a series of pronounced biotic and environmental changes at both global and regional scales, culminating in the end-Permian mass extinction (Shen et al., 2019). In the studied sections, the first occurrence of *Clarkina wangi* within the upper Dalong Formation indicates close proximity to the Wuchiapingian–Changhsingian boundary. Minor co-occurrences of *C. wangi* and *C. subcarinata* observed in the Huangping section are interpreted as the result of local ecological heterogeneity or preservational biases rather than as reflecting departures from the established global stratigraphic sequence (Fig. 4). Comparison among the three sections shows that the first appearance of *C. wangi* is broadly consistent in the Longmenba and Huangping sections, although minor differences in its exact stratigraphic position can be attributed to local lithologic variations within the upper Dalong Formation. In the Tongmuyuan section, *C. wangi* has not been directly recovered; nevertheless, correlation based on overlying diagnostic conodont taxa and lithostratigraphic similarity supports the presence of the Wuchiapingian–Changhsingian boundary in this section. Collectively, these observations support the interpretation of a broadly continuous Wuchiapingian–Changhsingian succession across all three sections despite local preservation or sampling limitations at Tongmuyuan. Among them, the Longmenba section provides the most complete record, allowing the most confident placement of the Wuchiapingian–Changhsingian boundary. Notably, siliceous shales in the study area do not extend upward to the Wuchiapingian–Changhsingian boundary. Their uppermost occurrences remain stratigraphically below the boundary horizon, as constrained by conodont biostratigraphy (Fig. 13).

6.2 The age of the shale gas “sweet spot” in the WHEC area

During the Lopingian, two major depositional troughs developed within the WHEC area: the Chengkou-Exi Trough and the Kaijiang-Liangping Trough (Fig. 1c). Although these

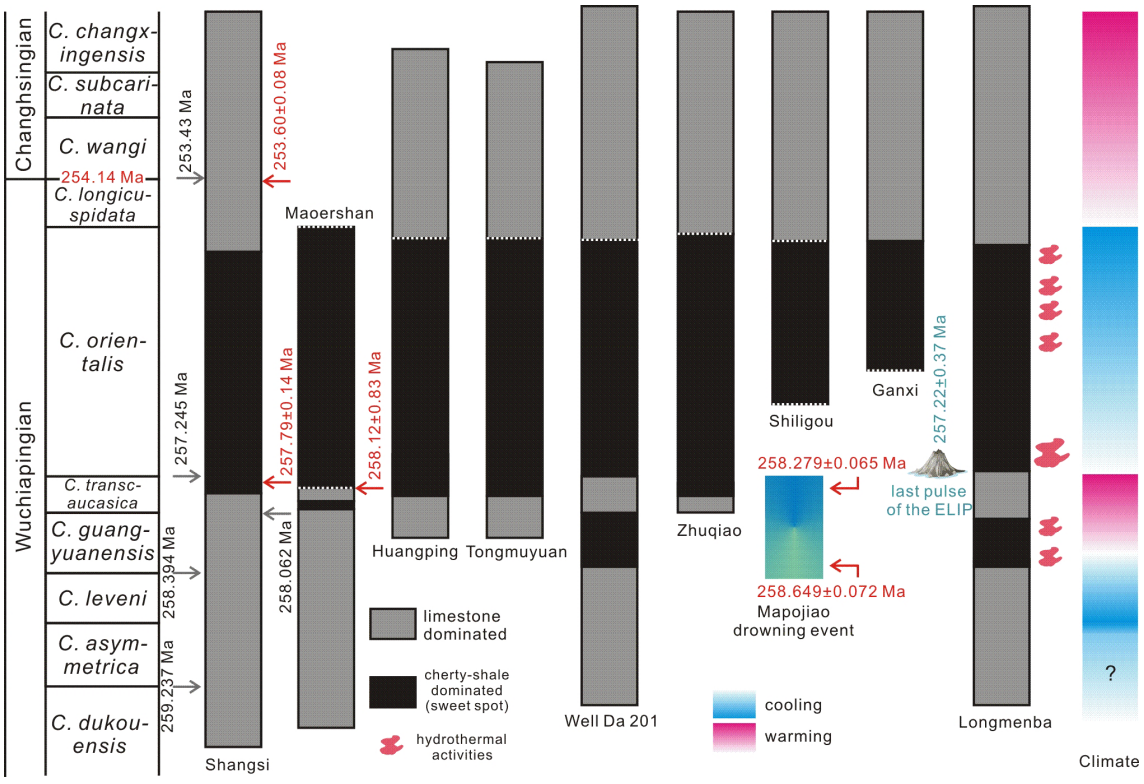

Figure 13. Conodont biozonation and key controlling factors for shale gas "sweet-spot" development in the WHEC area. Hydrothermal records are from the Longmenba section (Xu et al., 2025). The Mapojiao drowning event and related age constrains are from Bagherpour et al. (2018a, 2025). Numerical age for the base of the Changhsingian is from Ramezani and Bowring (2018). Red numerical data for the Shangsi section are based on U–Pb zircon dating (Shen et al., 2011), whereas gray numerical ages represent the 405 kyr-tuned astronomical timescale of Yuan et al. (2019). Red numerical ages for the Maoershan section are from Zhong et al. (2020). Age constraints on the termination of the Emeishan Large Igneous Province (LIP) are from Huang et al. (2022). Conodont biostratigraphic data are compiled from Yuan et al. (2019) for the Shangsi section, from Yong et al. (2025) for Well Da 201, from Zhong et al. (2020) for the Maoershan section, from Yang et al. (2019) for the Zhuqiao and Shiligou sections, and from Nafi et al. (2006) for the Ganxi section. Dashed lines between dark- and gray-shaded rectangles indicate uncertainty in the precise positions of conodont-zone boundaries.

troughs were partially separated by a low-relief slope between Liangping and Wanzhou, broadly comparable sedimentary successions accumulated in both depocenters during the Lopingian, particularly during deposition of the Dalong Formation (Yong et al., 2025). Recent exploration has demonstrated stable industrial-scale shale gas production in the WHEC area, especially in the Hongxing area within the Chengkou–Exi Trough (Hu et al., 2023; Yong et al., 2025). Among the vertically stacked shale intervals in the Permian succession, the first member of the Dalong Formation has been confirmed to be the most favorable shale gas target (Li et al., 2024). This unit conformably overlies the carbonate-dominated Xiayao Formation and is overlain by the muddy-limestone-dominated upper part of the Dalong Formation (Fig. 13; Li et al., 2024; Yong et al., 2025). Despite its economic importance, the precise chronostratigraphic position of this shale-gas-enriched interval has remained insufficiently constrained.

Based on the refined conodont biostratigraphic framework established in this study, the age of the shale gas "sweet spot" within the Dalong Formation of the WHEC area can now be more tightly constrained (Fig. 13). Integration of conodont zonations from the Longmenba, Huangping, and Tongmuyuan sections indicates that the gas-productive interval corresponds mainly to the upper part of the *Clarkina guangyuanensis* Zone and extends upward into the *C. orientalis* Zone or the lower *C. longicuspidata* Zone. This stratigraphic placement constrains the development of the shale gas sweet spot to the late Wuchiapingian, preceding the establishment of fully developed Changhsingian conodont assemblages.

Comparable age constraints have also been reported from other shale-gas-bearing successions in both depositional troughs. In the Shangsi section of the Kaijiang–Liangping Trough (Yuan et al., 2019), as well as in the Maoershan, Zhuqiao, Shiligou, and Ganxi sections and Well Da 201 from the Chengkou–Exi Trough (Nafi et al., 2006; Yang et al.,

2019; Zhong et al., 2020; Yong et al., 2025), gas-enriched shale horizons are predominantly associated with the *Clarkina orientalis* Zone and locally extend into the upper *C. transcaucasica* Zone (Fig. 13). Notably, Well Da 201 also records a gas-enriched shale interval within the upper *C. liangshanensis* Zone, which broadly corresponds to the *C. guangyuanensis* Zone in other sections (Fig. 13; Yuan et al., 2019).

Taken together, these observations indicate that shale gas enrichment in the WHEC region was not randomly distributed through time but instead was preferentially concentrated during the late Wuchiapingian (Fig. 13). This interval coincides with the deposition of organic-rich, siliceous shales of the lower Dalong Formation under relatively stable deep-water conditions. In contrast, the overlying Changhsingian succession records changes in sedimentary facies and paleoenvironmental regimes that were less favorable for sustained organic matter accumulation and shale gas preservation. Accordingly, the late Wuchiapingian represents a critical stratigraphic window for shale gas "sweet-spot" development in the WHEC region.

6.3 Depositional and paleoenvironmental controls on shale gas "sweet-spot" development

The temporal restriction of shale gas enrichment to the late Wuchiapingian in the WHEC region indicates that the development of the shale gas "sweet spot" was not accidental but instead resulted from a specific combination of depositional and paleoenvironmental conditions operating during this interval. These conditions reflect the coupled effects of regional basin evolution and broader Lopingian environmental changes. The high-resolution conodont biostratigraphic framework established in this study provides a critical temporal constraint, allowing depositional processes and paleoenvironmental events in the WHEC region to be evaluated in a robust chronostratigraphic context and compared directly with coeval successions in South China and elsewhere.

Water depth exerted a first-order control on the development of shale gas–favorable facies. Paleogeographic reconstructions indicate that the end-Guadalupian regression culminated during the *Clarkina leveni* Zone, corresponding to the first 1–2 Myr of the early Wuchiapingian (Yuan et al., 2019; Hou et al., 2020; Shen et al., 2023). Following this regression, renewed basin subsidence led to the development of at least two deep-water depocenters in the Middle and Upper Yangtze region at approximately 258 Ma, broadly coincident with the *C. guangyuanensis* Zone (Yuan et al., 2019; Hou et al., 2020). In the Well Da 201, as well as in the Maoershan and Longmenba sections, cherty-shale-dominated sedimentation initiated within the *C. guangyuanensis* Zone or the overlying *C. transcaucasica* Zone, both of which represent temporally short but stratigraphically significant intervals within the late Wuchiapingian (Yuan et al., 2019; Yong et al., 2025). From this time until the end of the Wuchiapingian, the WHEC region occupied a relatively deep-water depositional setting characterized by reduced terrigenous clastic input, enhanced silica accumulation, and persistent water column stratification (Fig. 13; Xu et al., 2025; Yu et al., 2025). Those are widely regarded to be favorable for elevated primary productivity in surface waters and for efficient preservation of organic matter at the seafloor. Together, they provided a sedimentary and geochemical framework conducive to the accumulation of organic-rich, cherty shales within the lower Dalong Formation. The close stratigraphic correspondence between the onset of siliceous-shale deposition and late Wuchiapingian conodont zones highlights the strong linkage between basin deepening and shale gas sweet-spot development (Yong et al., 2025; Xu et al., 2025).

At a broader scale, the late Wuchiapingian corresponds to a critical phase of global environmental reorganization associated with the transition from the Late Paleozoic icehouse to the Mesozoic greenhouse climate system (Fielding et al., 2008). Geochemical evidence suggests that Lopingian seawater temperatures were generally higher than those of the Cisuralian and Guadalupian (Chen et al., 2013). However, conodont apatite oxygen isotope data indicate that the early Lopingian was punctuated by superimposed short-term cooling episodes (Chen et al., 2013; Yang et al., 2015). Subsequent studies based on oxygen isotope records from both conodont apatite and brachiopod calcite further demonstrate that the *Clarkina leveni* and *C. orientalis* zones were associated with relatively cooler climatic conditions (Wang et al., 2020; Viaretti et al., 2025). These cooling intervals may have enhanced vertical mixing and nutrient recycling, thereby promoting biogenic silica production and organic matter preservation in deep-water basins (Xu et al., 2025). As estimated by Yuan et al. (2019), the duration of the *C. orientalis* Zone accounts for nearly half of the Wuchiapingian, indicating that the shale-gas-favorable depositional regime persisted over a sufficiently long time span to allow the accumulation of thick, laterally extensive organic-rich shales. Consequently, the shale gas "sweet spot" of the WHEC region can be interpreted as the product of a temporally focused but environmentally stable interval during the late Wuchiapingian, when basin geometry, sea level configuration, and climate-modulated oceanographic conditions collectively favored organic matter enrichment (Xu et al., 2025).

6.4 Temporal overlap between late Wuchiapingian volcanism and shale gas "sweet-spot" deposition in the WHEC area

The temporal coincidence between shale gas "sweet-spot" development and the late Wuchiapingian is noteworthy and invites consideration of potential links with large-scale tectono-magmatic processes, particularly the waning eruptive phase of the Emeishan LIP. However, temporal overlap alone does not establish a direct causal relationship, and any proposed volcanic influence must be evaluated within the

broader framework of basin evolution and paleoceanographic change.

Although estimates for the total duration of the Emeishan LIP vary widely (e.g., 271–235 Ma), high-precision CA-ID-TIMS geochronological data from southwestern China and northern Vietnam constrain the main eruptive phase to a relatively short interval between 260.55 and 257.22 Ma, extending into the Wuchiapingian Stage (Yang et al., 2015; Shellnutt et al., 2020; Huang et al., 2022). Evidence for continued volcanic activity during the late Wuchiapingian has also been reported from the Shuanghe section within the Chengkou–Exi Trough, where felsic volcanic ash layers from the lower Dalong Formation yielded an LA-ICP-MS U–Pb zircon age of 253 ± 3.1 Ma (Li et al., 2022). Although this age potentially overlaps with the Changhsingian, integration with the refined conodont biostratigraphy established in this study suggests that these ash layers most likely correspond to the Wuchiapingian interval.

Additional support for episodic volcanic activity during the Wuchiapingian is provided by in situ U–Pb geochronological data from Guadalupian giant-bivalve-bearing successions, which indicate multiple small-scale eruptive pulses during the waning stage of the Emeishan LIP (Zhao et al., 2026). Stratigraphic correlations from the Maoershan and Chaotian sections, located in the two major depositional troughs, further suggest that volcanic activity persisted until approximately 257.4 Ma, stratigraphically above the *Clarkina transcaucasica* Zone but below the *C. orientalis* Zone (Fig. 13; Zhong et al., 2020). Moreover, data from the Xikou section, situated on a terrane accreted to the North China Block and separated from the South China Block by the Mianlue Ocean, indicate that the final eruptive pulses of the Emeishan LIP may have extended into the *C. liangshanensis* or even the *C. orientalis* Zone (Cheng et al., 2025).

A drowning event during the Wuchiapingian has been independently documented at the Mapojiao section in Guizhou Province, spanning the *Clarkina guangyuanensis* to *C. transcaucasica* zones (Bagherpour et al., 2018a). This interval was subsequently formalized as the "Mapojiao Event" and interpreted as a response to environmental perturbations associated with pulses of Emeishan LIP volcanism (Bagherpour et al., 2018b, 2025). In the Longmenba section of the WHEC area, the cherty-shale-dominated interval of the Dalong Formation likewise contains abundant volcanic ash layers, demonstrating that deep-water deposition occurred contemporaneously with volcanic input (Xu et al., 2025).

Collectively, these lines of evidence indicate that multiple volcanic pulses associated with the waning phase of the Emeishan LIP temporally overlapped with deposition of the shale gas "sweet-spot" interval within the Dalong Formation of the WHEC area. Nevertheless, basin deepening, enhanced silica accumulation, and associated paleoceanographic conditions likely exerted a primary control on organic matter accumulation and preservation. Volcanism may have acted as an external modulating factor by influencing regional climate, weathering fluxes, nutrient delivery, and silica cycling, thereby indirectly enhancing conditions favorable for organic-rich shale formation (Xu et al., 2025). In this framework, late Wuchiapingian magmatic activity is interpreted as a plausible secondary contributing factor rather than a principal driver of shale gas "sweet-spot" development.

7 Conclusions

1. A high-resolution conodont biostratigraphic framework is established for the upper Permian (latest Guadalupian–Lopingian) successions of the WHEC area, documenting a near-continuous record from the late Guadalupian through the Changhsingian. The recognized zonal sequence closely matches the GSSP-calibrated conodont framework of South China and provides a robust basis for regional and interbasinal correlation.

2. The Wuchiapingian–Changhsingian boundary can be placed using conodont biostratigraphy, primarily based on the first appearance of *Clarkina wangi*. Local absences of key taxa in some sections are best explained by lithofacies control and preservation bias rather than by major stratigraphic discontinuities.

3. Organic-rich siliceous shales of the lower Dalong Formation are temporally restricted to the late Wuchiapingian, corresponding mainly to the upper *Clarkina guangyuanensis* Zone and extending into the *C. orientalis* or lowermost *C. longicuspidata* Zone. This demonstrates that shale development is confined to a specific and narrowly defined biostratigraphic interval.

4. The temporal coincidence between late Wuchiapingian conodont zones and waning volcanic activity of the Emeishan Large Igneous Province suggests that large-scale tectono-magmatic processes may have indirectly influenced regional depositional environments and biotic distributions during this interval.

5. This study underscores the central role of conodont biostratigraphy in resolving Lopingian stratigraphic architecture and paleoenvironmental evolution, demonstrating how micropaleontological data can provide precise temporal constraints for interpreting sedimentary processes in complex basin systems.

Data availability. The material can be accessed at the Hubei Institute of Geosciences, Wuhan, China.

Author contributions. BYZ: writing (original draft), investigation, data curation. KW: writing (original draft, review and editing), supervision, investigation, formal analysis, data curation. TS: writing (review and editing), data curation. LLX: writing (review and

editing), data curation. KD: writing (review and editing), data curation. JLY: writing (review and editing), data curation. LZY: writing (review and editing), data curation. BZ: writing (review and editing), data curation. JLL: writing (review and editing), investigation. DW: review, editing, investigation. BYY: writing (review and editing), supervision, investigation.

Competing interests. The contact author has declared that none of the authors has any competing interests.

Disclaimer. Publisher's note: Copernicus Publications remains neutral with regard to jurisdictional claims made in the text, published maps, institutional affiliations, or any other geographical representation in this paper. The authors bear the ultimate responsibility for providing appropriate place names. Views expressed in the text are those of the authors and do not necessarily reflect the views of the publisher.

Acknowledgements. We thank Wei Wang, Yasheng Cui, and Haoyu Yu (HIG), as well as Qiuchen Xu and Yuluo Wang (OGS), for their assistance during the fieldwork. We are further grateful to Mingling Li (HMU) for providing part of the sample material and to Dan Zhu (HGRL) for the assistance with the SEM analyses.

Financial support. This research was supported by the Natural Science Foundation of Hubei Province (grant no. 2024AFD394) and the Science and Technology Special Fund of the Hubei Geological Bureau (grant nos. KJ2025-4 and KJ2026-4).

Review statement. This paper was edited by Maria Rose Petrizzo and reviewed by two anonymous referees.

References

Bagherpour, B., Bucher, H., Yuan, D. X., Leu, M., Zhang, C., and Shen, S. Z.: Early Wuchiapingian (Lopingian, late Permian) drowning event in the South China block suggests a late eruptive phase of Emeishan large Igneous Province, Global Planet. Change, 19, 119–132, https://doi.org/10.1016/j.gloplacha.2018.07.013, 2018a.

Bagherpour, B., Bucher, H., Schneebeli-Hermann, E., Vennemann, T., Chiaradia, M., and Shen, S. Z.: Early Late Permian coupled carbon and strontium isotope chemostratigraphy from South China: Extended Emeishan volcanism?, Gondwana Res., 58, 58–70, https://doi.org/10.1016/j.gr.2018.01.011, 2018b.

Bagherpour, B., Lena, L., Ovtcharova, M., Yuan, D. X., Shen, S. Z., Bucher, H., and Schaltegger, U.: Correlating early Wuchiapingian (early Lopingian/late Permian) biotic and environmental changes with eruptive activity of the Emeishan LIP, Lithios, 494–495, 107937, https://doi.org/10.1016/j.lithos.2024.107937, 2025.

Chen, B., Joachimski, M. M., Shen, S. Z., Lambert, L. L., Lai, X. L., Wang, X. D., Chen, J., and Yuan, D. X.: Permian ice volume and palaeoclimate history: Oxygen isotope proxies revisited, Gondwana Res., 24, 77–89, https://doi.org/10.1016/j.gr.2012.07.007, 2013.

Cheng, C., Zhang, H., Wang, D., Li, S. Y., and Shen, S. Z.: Pulsed volcanism in the Emeishan Large Igneous Province drove deglaciation during the Guadalupian-Lopingian transition, Palaeogeogr. Palaeocl., 679, 113302, https://doi.org/10.1016/j.palaeo.2025.113302, 2025.

Du, M. Y., Wu, K., Huang, Y. F., Yang, B. Y., Yang, L. Z., Wang, Y. D., Zhao, J. J., Li, M. F., and Huang, Z. H.: Conodont biostratigraphy around the Permian-Triassie boundary from the Jianzishan section, Lichuan, Hubei Province, and its implicationsfor the age of microbialites, Acta Geol. Sin., 99, 2204–2216, 2025 (in Chinese with English abstract).

Fan, J. X., Shen, S. Z., Erwin, D. H., Sadler, P. M., Macleod, N., Cheng, Q. M., Hou, X. D., Yang, J., Wang, X. D., Wang, Y., Zhang, H., Chen, X., Li, C., and Zhao, Y. Y.: A high-resolution summary of Cambrian to Early Triassic marine invertebrate biodiversity, Paleontology, 367, 272–277, 2020.

Fielding, C. R., Frank, T. D., Birgenheier, L. P., Rygel, M., Jones, A. T., and Roberts, J.: Stratigraphic imprint of the Late Paleozoic Ice Age in eastern Australia: A record of alternating glacial and nonglacial climate regime, J. Geol. Soc., 165, 129–140, https://doi.org/10.1144/0016-76492007-036, 2008.

Gong, Z., Crowley, J. L., Kamo, S. L., Denyszn, S. W., Zhang, M. C., Li, J., Liu, Y. M., and Huang, C. M.: Protracted post–eruptive basaltic weathering of the Emeishan large igneous province constrained by U–Pb CA–ID–TIMS geochronology, Palaeogeogr. Palaeocl., 659, 112666, https://doi.org/10.1016/j.palaeo.2024.112666, 2025.

Gullo, M. and Kozur, H. W.: Conodonts from the pelagic deep-water Permian of central western Sicily (Italy), Neues Jahrb. Geol. P., 184, 203–234, 1992.

Guo, X. S., Wang, R. Y., Shen, B. J., Wang, G. P., Wan, C. X., and Wang, Q. R.: Geological characteristics, resource potential, and development direction of shale gas in China, Petrol. Explor. Dev., 52, 17–32, https://doi.org/10.1016/S1876-3804(25)60002-4, 2025.

Henderson, C. M.: Permian conodont biostratigraphy, Geol. Soc. Lond. Spec. Publ., 450, 119–142, https://doi.org/10.1144/SP450.9, 2018.

Hou, Z. S., Fan, J. X., Henderson, C. M., Yuan, D. X., Shen, B. H., Wu, J., Wang, Y., Zheng, Q. F., Zhang, Y. C., Wu, Q., and Shen, Z.: Dynamic palaeogeographic reconstructions of the Wuchiapingian Stage (Lopingian, Late Permian) for the South China Block, Palaeogeogr. Palaeocl., 546, 109667, https://doi.org/10.1016/j.palaeo.2020.109667, 2020.

Hu, D. G., Zhou, L., Bao, H. Y., Liu, H. T., Liu, C., Meng, Z. Y., Zhao, S., and Wang, J.: Breakthrough and significance of Permian shale gas exploration of Well HY1 in Hongxing area, eastern Sichuan Basin, Acta Petrol. Sin., 44, 241–252, https://doi.org/10.7623/syxb202302002, 2023 (in Chinese with English abstract).

Huang, H., Huyskens, M. H., Yin, Q. Z., Cawood, P. A., Hou, M. C., Yang, J. H., Xiong, F. H., Du, Y. S., and Yang, C. C.: Eruptive tempo of Emeishan large igneous province, southwestern China and northern Vietnam: Relations to biotic crises and paleoclimate

changes around the Guadalupian-Lopingian boundary, Geology, 50, 1083–1087, https://doi.org/10.1130/G50183.1, 2022.

Jin, Y. G., Shen, S. Z., Henderson, C. M., Wang, X. D., Wang, W., Wang, Y., Cao, C. Q., and Shang, Q. H.: The Global Stratotype Section and Point (GSSP) for the boundary between the Capitanian and Wuchiapingian Stage (Permian), Episodes, 29, 253–262, 2006a.

Jin, Y. G., Wang, Y., Henderson, C., Wardlaw, B. R., Shen, S. Z., and Cao, C. Q.: The Global Boundary Stratotype Section and Point (GSSP) for the base of Changhsingian Stage (Upper Permian), Episodes, 29, 175–182, 2006b.

Kozur, H. W.: Beitrage zur conodontenfauna des Perm, Geologische Palaontologische Mitteilungen Innsbruck, 5, 1–44, 1975.

Kozur, H. W.: Pelagic uppermost Permian and the Permian–Triassic boundary conodonts of Iran. Part II: investigated sections and evaluation of the conodonts fanuas, Hallesches Jahrbuch Geowiss, Reihe B, Beiheft, 19, 49–86, 2005.

Li, M. L., Yang, B. Y., Qiu, L., Zhang, Y. J., Xu, H., Shi, X. B., Tian, W. X., Wang, Y., Gao, J., and Zheng, D. S.: Emeishan felsic volcanism lasted until the Changhsingian? New evidence from volcanic ash in the northern South China block, J. Asian Earth Sci., 238, 105390, https://doi.org/10.1016/j.jseaes.2022.105390, 2022.

Li, S. Z., Yang, X. G., Xu, Q. C., Li, F., Song, T., Li, H. H., Wei, S. Y., Wang, C., and Wang, Y. L.: Permian Dalong Formation – a new formation for shale gas exploration and development, Geol. Rev., 70, 253–254, http://https://doi.org/10.16509/j.georeview.2024.s1.137, 2024 (in Chinese with English abstract).

Li, Z. S., Zhan, L. P., Dai, J. Y., Jin, R. G., Zhu, X. F., Zhang, J. H., Huang, H. Q., Xu, D. Y., Yan, Z., and Li, H. M.: Study on the Permian–Triassic Biostratigraphy and Event Stratigraphy of Northern Sichuan and Southern Shaanxi, Geological Publishing House, Beijing, 435, 1989 (in Chinese with English abstract).

Lyu, Z. Y., Orchard, M. J., Chen, Z. Q., Wang, X. D., Zhao, L. S., and Han, C.: Uppermost Permian to Lower Triassic conodont successions from the Enshi area, western Hubei Province, South China, Palaeogeogr. Palaeocl., 519, 49–64, https://doi.org/10.1016/j.palaeo.2017.08.015, 2019.

Mei, S. L., Jin, Y. G., and Wardlaw, B. R.: Succession of Conodonts Zones From The Permian "Kuhfeng" Formation, Xuanhan, Sichuan, And Its Implication In Global Correlation, Acta Palaeontol. Sin., 33, 1–23+131–133, https://doi.org/10.19800/j.cnki.aps.1994.01.001, 1994a (in Chinese with English abstract).

Mei, S. L., Jin, Y. G., and Wardlaw, B. R.: Succession of Wuchiapingian Conodonts From Northeastern Sichuan And Its Worldwide Correlation, Acta Micropalaeontologica Sinica, 11, 121–139, 1994b.

Mei, S. L., Jin, Y. G., and Wardlaw, B. R.: Zonation Of Conodonts Form The Maokouan–Wuchiapingian Boundary Strata, South China, Palaeoworld, 4, 225–233, 1994c.

Mei, S. L., Henderson, C. M., and Cao, C. Q.: Conodont sample-population approach to defining the base of the Changhsingian Stage, Lopingian Series, Upper Permian, Geol. Soc. Lond. Spec. Publ., 230, 105–121, 2004.

Meng, Q., Xue, W.Q., Chen, F. Y., Yan, J. X., Cai, J. H., Sun, Y. D., Wignall, P. B., Liu, K., Liu, Z. C., and Chen, D.: Stratigraphy of the Guadalupian (Permian) siliceous deposits from central Guizhou of South China: Regional correlations with implications for carbonate productivity during the Middle Permian biocrisis, Earth Sci. Rev., 228, 104011, https://doi.org/10.1016/j.earscirev.2022.104011, 2022.

Metcalfe, I. and Crowley, J. L.: Upper Permian and Lower Triassic conodonts, high-precision U-Pb zircon ages and the Permian-Triassic boundary in the Malay Peninsula, J. Asian Earth Sci., 199, 104403, https://doi.org/10.1016/j.jseaes.2020.104403, 2020.

Nafi, M., Xia, W. C., and Zhang, N.: Late Permian (Changhsingian) conodont biozonation and the basal boundary, Ganxi section, western Hubei Province, south China, Can. J. Earth Sci., 43, 121–133, https://doi.org/10.1139/E05-097, 2006.

Qiu, Z., Dou, L. R., Wu, J. F., Wei, H. Y., Liu, W., Kong, W. L., Zhang, Q., Cai, G. Y., Zhang, G., Wu, W., Li, S. Z., Qu, T. Q., and Gao, W. L.: Lithofacies Palaeogeographic Evolution of the Middle Permian Sequence Stratigraphy and Its Implications for Shale Gas Exploration in the Northern Sichuan and Western Hubei Provinces, Earth Sci., 49, 712–748, https://doi.org/10.3799/dqkx.2023.216, 2024.

Ramezani, J. and Bowring, S. A.: Advances in numerical calibration of the Permian timescale based on radioisotopic geochronology, Geol. Soc. Lond. Spec. Publ., 450, 51–60, https://doi.org/10.1144/SP450.17, 2018.

Shellnutt, J. G., Pham, T. T., Denyszyn, S. W., Yeh, M. W., and Tran, T. A.: Magmatic duration of the Emeishan large igneous province: insight from northern Vietnam, Geology, 48, 457–461, https://doi.org/10.1130/g47076.1, 2020.

Shen, S. Z.: The Permian GSSPs and timescale: Progress, unsolved problems and perspectives, Permophiles, 75, 12–18, 2023.

Shen, S. Z. and Mei, S. L.: Lopingian (Late Permian) high-resolution conodont biostratigraphy in Iran with comparison to South China zonation, Geol. J., 45, 135–161, https://doi.org/10.1002/gj.1231, 2010.

Shen, S. Z., Crowley, J. L., Wang, Y., Bowring, S. A., Erwin, D. H., Sadler, P. M., Cao, C. Q., Rothman, D. H., Henderson, C. M., Ramezani, J., Zhang, H., Shen, Y., Wang, X. D., Wang, W., Mu, L., Li, W. Z., Tang, Y. G., Liu, X. L., Liu, L. J., Zeng, Y., Jiang, Y. F., and Jin, Y. G.: Calibrating the End-Permian Mass Extinction, Science, 334, 1367–1372, https://doi.org/10.1126/science.1213454, 2011.

Shen, S. Z., Zhang, H., Zhang, Y. C., Yuan, D. X., Chen, B., He, W. H., Mu, L., Lin, W., Wang, W. Q., Chen, J., Wu, Q., Cao, C. Q., Wang, Y., and Wang, X. D.: Permian integrative stratigraphy and timescale of China, Sci. China Earth Sci., 62, 154–188, https://doi.org/10.1007/s11430-017-9228-4, 2019.

Shen, S. Z., Yuan, D. X., Zhang, Y. C., Henderson, C. M., Zheng, Q. F., Zhang, H., Zhang, M., Dai, Y., Xu, H. P., Wang, W. Q., Li, Q., Wang, Y., Wang, X. D., Mu, L., Ramenzani, J., Erwin, D. H., Angiolini, L., Zhang, F. F., Hou, Z. S., Chen, J., Zhang, X. Y., Zhang, S. H., Wu, Q., Pan, Y. X., Stephenson, M., and Mei, S. L.: Redefinition of the Global Stratotype Section and Point (GSSP) and new Standard Auxiliary Boundary Stratotype (SABS) for the base of Wuchiapingian Stage (Lopingian Series, Permian) in South China, Episodes, 47, 147–177, https://doi.org/10.18814/epiiugs/2023/023023, 2023.

Viaretti, M., Crippa, G., Brombin, V., Porta, G. D., Griesshaber, E., Jurikova, H., Posenato, R., Bottini, C., and Angiolini, L.: Duration and intensity of the Late Permian (early Wuchiapingian)

cool climate episode: Sclerochemical evidence from brachiopod assemblages in Iran, Palaeogeogr. Palaeocl., 659, 112654, https://doi.org/10.1016/j.palaeo.2024.112654, 2025.

Wang, C. Y. and Dong, Z. C.: Permian conodonts from Suoxiyu in Cili County, Hunan, Acta Micropalacontologica Sinica, 8, 41–56, 1991 (in Chinese with English abstract).

Wang, C. Y. and Wang, Z. H.: Permian conodont biostratigraphy of China, Geol. Soc. Am. S., 187, 227–236, 1981a.

Wang, C. Y. and Wang, Z. H.: Permian conodonts from the Longtan Formation and Changxing Formation of Changxing, Zhejiang and their stratigraphical and palaeoecological significance, Selected Papers of 1st Convention Micropaleontological Society of China, 114–120, 1981b (in Chinese with English abstract).

Wang, W. Q., Garbelli, C., Zhang, F. F., Zheng, Q. F., Zhang, Y. C., Yuan, D. X., Shi, Y. K., Chen, B., and Shen, S. Z.: A high-resolution Middle to Late Permian paleotemperature curve reconstructed using oxygen isotopes of well-preserved brachiopod shells, Earth Planet. Sc. Lett., 540, 116245, https://doi.org/10.1016/j.epsl.2020.116245, 2020.

Wang, Z. H.: Permian–Lower Triassic conodonts of the Liangshan area, southern Shaanxi, Acta Palaeotologica Sinica, 17, 213–232, 1978 (in Chinese with English abstract).

Wignall, P. B., Sun, Y. D., Bond, D. P. G., Izon, G., Newton, R. J., Védrine, S., Widdowson, M., Ali, J. R., Lai, X. L., Jiang, H. S., Cope, H., and Bottrell, S. H.: Volcanism, Mass Extinction, and Carbon Isotope Fluctuations in the Middle Permian of China, Science, 324, 1179–1182, 2009.

Wu, G. C., Ji, Z. S., Lash, G. G., Yao, J. X., Zhang, S. W., and Li, Y. X.: Newly discovered Wuchiapingian to Olenekian conodonts from the Longgar area, southern Lhasa Terrane and their palaeobiogeographical implications, Lethaia, 54, 723–735, https://doi.org/10.1111/let.12435, 2021.

Xu, L. L., Huang, S. P., Liu, D. M., Liao, Z. W., Wu, K., Chen, M. K., Zhou, X. H., Zhang, Y. L., Liu, B., and Li, M.: Extensive accumulation of organic matter in the Late Permian Dalong Formation, Western Hubei Trough, Southern China, International Journal of Coal Geology, 302, 104727, https://doi.org/10.1016/j.coal.2025.104727, 2025.

Yang, B., Li, H. X., Wignall, P. B., Jiang, H. S., Niu, Z. J., Ye, Q., Wu, Q., and Lai, X. L.: Latest Wuchiapingian to Earliest Triassic Conodont Zones and $\delta^{13}C_{carb}$ Isotope Excursions from Deep-Water Sections in Western Hubei Province, South China, J. Earth Sci., 30, 1059–1074, https://doi.org/10.1007/s12583-019-1018-2, 2019.

Yang, J. H., Cawood, P. A., and Du, Y. S.: Voluminous silicic eruptions during late Permian Emeishan igneous province and link to climate cooling, Earth Planet. Sc. Lett., 432, 166–175, https://doi.org/10.1016/j.epsl.2015.09.050, 2015.

Yin, H. F., Zhang, K. X., Tong, J. N., Yang, Z. Y., and Wu, S. B.: The Global Stratotype Section and Point (GSSP) of the Permian-Triassic Boundary, Episodes, 24, 102–114, 2001.

Yong, R., Yang, H. Z., Wu, W., Yang, X., Yang, Y. R., and Huang, H. Y.: Controlling factors and exploration potential of shale gas enrichment and high yield in Permian Dalong Formation, northern Sichuan Basin, SW China, Petrol. Explor. Dev., 52, 285–300, https://doi.org/10.1016/S1876-3804(25)60567-2, 2025.

Yu, M. X., Zhao, J. H., Liu, K. Y., Hu, Q. H., Wu, W., Liu, Q. Y., Luo, C., Chen, Y., Ma, H. Y., and Jin, Z. J.: Paleoenvironment and organic matter enrichment in the Kaijiang–Liangping Trough across the Emeishan Large Igneous Province (ELIP), Mar. Petrol. Geol., 181, 107517, https://doi.org/10.1016/j.marpetgeo.2025.107517, 2025.

Yuan, D. X., Shen, S. Z., Henderson, C. M., Chen, J., Zhang, H., and Feng, H. Z.: Revised conodont-based integrated high-resolution timescale for the Changhsingian Stage and end-Permian extinction interval at the Meishan sections, South China, Lithos, 204, 220–245, https://doi.org/10.1016/j.lithos.2014.03.026, 2014.

Yuan, D. X., Shen, S. Z., and Henderson, C. M.: Revised Wuchiapingian conodont taxonomy and succession of South China, J. Paleontol., 91, 1191–1219, https://doi.org/10.1017/jpa.2017.71, 2017.

Yuan, D. X., Shen, S. Z., Henderson, C. M., Chen, J., Zhang, H., Zheng, Q. F., and Wu, H. C.: Integrative timescale for the Lopingian (Late Permian): A review and update from Shangsi, South China, Earth-Sci. Rev., 188, 190–209, https://doi.org/10.1016/j.earscirev.2018.11.002, 2019.

Yuan, D. X., Zhang, Y. C., Gorgij, M. N., Zhang, H., Angiolini, L., Crippa, G., Chen, J., and Shen, S. Z.: Lopingian biotic crisis and global correlation: Evidence from the Abadeh section, central Iran, Palaeogeography, Palaeoclimatology, Palaeoecology, 677, 113211, https://doi.org/10.1016/j.palaeo.2025.113211, 2025.

Zhang, K. X.: The Permo-Triassic conodont fauna in Changxing area, Zhejiang Province and its stratigraphic significance, Earth Sci., 12, 193–200, 1987.

Zhang, L. L., Zhang, N., and Xia, W. C.: Conodont succession in the Guadalupian–Lopingian boundary interval (upper Permian) of the Maoershan section, Hubei Province, China, Micopaleontology, 53, 433–446, 2007.

Zhang, L., Wu, J., Yuan, D. X., Forel, M. B., Chang, S., Khan, M. Z., Feng, Q. L., He, W. H., Ma, Q. F., Danelian, T., Caridroit, M., and Tsuyoshi, I.: Integrated Radiolarian and Conodont Biostratigraphy of the Middle to Late Permian Linghao Formation in Northwestern Guangxi, South China, Acta Geol. Sin.-Engl., 95, 1984–1997, https://doi.org/10.1111/1755-6724.14721, 2021.

Zhang, S. H., Yuan, D. X., and Shen, S. Z.: Global correlation of the Guadalupian–Lopingian transition and associated events using a quantitative conodont-based biostratigraphic scheme, Palaeogeogr. Palaeocl., 655, 112502, https://doi.org/10.1016/j.palaeo.2024.112502, 2024.

Zhang, S. H., Zhao, Y. Y., Shi, Y. K., Fang, Q., Wang, X. D., Fan, J. X., Zhang, Y. C., Yuan, D. X., Wang, Y., Zhang, F. F., Wu, H. C., Erwin, D. H., Marshall, C. R., and Shen, S. Z.: Global cooling drove diversification and warming caused extinction among Carboniferous–Permian fusuline foraminifera, Sci. Adv., 11, 2549, https://doi.org/10.1126/sciadv.adv2549, 2025a.

Zhang, X., Wei, H. Y., Wu, K., Gong, J. X., Wen, Y., and Mansour, A.: Marine redox evolutions and carbon isotope variations during the Guadalupian–Lopingian transition in the Yangtze Platform, South China, Palaeogeogr. Palaeocl., 660, 112681, https://doi.org/10.1016/j.palaeo.2024.112681, 2025b.

Zhao, X. Q., Liu, R., Wang, F. D., Li, Q., Su, C., Ding, J. M., Xiong, C. F., Li, W. T., Zhang, J. H., and Hou, K. L.: Determining the age of Guadalupian extinction by in situ uranium–lead geochronology in regard to middle Permian giant bivalve Alatoconchidae fossils in the Northwest margin of the South China Plate, Gondwana Res., 150, 405–418, https://doi.org/10.1016/j.gr.2025.10.008, 2026.

Zhong, Y. T., Mundil, R., Chen, J., Yuan, D. X., Denyszyn, S. W., Jost, A. B., Payne, J. L., He, B., Shen, S. Z., and Xu, Y. G.: Geochemical, biostratigraphic, and high-resolution geochronological constraints on the waning stage of Emeishan Large Igneous Province, Geol. Soc. Am., 132, 1969–1986, https://doi.org/10.1130/B35464.1, 2020.